

# Gradient elasticity in Swift-Hohenberg and phase-field crystal models

Lucas Benoit--Maréchal<sup>1</sup>, and Marco Salvalaglio<sup>1,2</sup>

<sup>1</sup>Institute of Scientific Computing, TU Dresden, 01062 Dresden, Germany.

<sup>2</sup>Dresden Center for Computational Materials Science, TU Dresden, 01062 Dresden, Germany.

E-mail: marco.salvalaglio@tu-dresden.de

**Abstract.** The Swift-Hohenberg (SH) and Phase-Field Crystal (PFC) models are minimal yet powerful approaches for studying phenomena such as pattern formation, collective order, and defects via smooth order parameters. They are based on a free-energy functional that includes elasticity with linear, nonlinear, and strain-gradient contributions. The latter is peculiar to gradient elasticity (GE), a theory that accounts for elasticity effects at microscopic scales by introducing additional characteristic lengths. While numerical simulations of SH and PFC models display some distinctive GE features, such as the regularization of stress singularities at crystalline defects, a comprehensive analysis has yet to be conducted. This study addresses how GE is incorporated into SH and PFC models. We calculate its characteristic lengths for various lattice symmetries in an approximated setting. We then discuss the effective elasticity theory encoded in SH and PFC models via numerical simulations of dislocation stress fields and comparisons with solutions within first and second strain GE. We then demonstrate that effective GE characteristic lengths depend on the free-energy parameters, similar to the correlation length, thus unveiling how they change with the quenching depth and the phenomenological temperature entering the considered models. The findings presented in this study enable a thorough discussion and analysis of small-scale elasticity effects in pattern formation using SH and PFC models and complete the elasticity analysis therein. Additionally, we provide a microscopic foundation for GE in the context of order-disorder phase transitions.

*Keywords:* gradient elasticity, pattern formation, phase-field crystal, lattice deformation, dislocations

## 1. Introduction

Gradient elasticity (GE) is a theoretical framework that extends classical continuum mechanics with additional higher-order derivatives to capture the effects of small length scales [1–5]. It incorporates additional characteristic lengths accounting for internal material structure and discreteness, thereby including size effects relevant at the nano- and micro-scale. Such a theory has been tested and exploited in different frameworks, e.g., classical mechanics and dislocation dynamics, and applied in contexts such as flexoelectricity and biomechanics [6–12]. It has also been extended to describe strain gradient plasticity [13–16]. Parameters entering the theory have been connected to interatomic potentials and, in general, can be determined by atomistic methods [17–19]. A key feature of GE is that it overcomes some limitations of continuum elasticity theory, such as unphysical singularities emerging from approximated descriptions of small scales. This leads, for instance, to regularized elastic fields at the dislocation core [20–23], which are instead singular in classic linear elasticity [24].

Elasticity-driven pattern formation emerges in physical systems due to the interplay between mechanical deformation and other physical contributions such as capillarity, solidification, crystal growth dynamics, and grand potential jumps across interfaces. This can occur in various systems such as hard and soft materials as well as biological tissues [25, 26]. Concerning the study of general features of pattern formation, a central role has been played by the so-called Swift-Hohenberg (SH) model [27, 28] and its extensions. It is based on a partial differential equation (the SH equation) that describes the spatiotemporal evolution of a real order parameter field,  $\psi$ , comprising linear differential operators and nonlinear polynomials. Such an equation favors the linear growth of periodic modes of  $\psi$ . At the same time, nonlinear terms lead to saturation of this growth and selection of patterns with different symmetry depending on parameters. Notably, the SH equation can be written in a variational form through the definition of a free energy (or Ljapunov) functional  $F[\psi]$  as  $\partial_t \psi = -\delta F / \delta \psi$ . Therefore, stable stationary states correspond to the minima of such functional. While it was initially proposed to model the so-called Rayleigh-Benard convection in a heated fluid, similar equations have been exploited to describe the emergence of patterns involving elasticity effects in different contexts [29–31]. The connection of SH-like models to elasticity became evident in the conservative formulation, the so-called phase field crystal (PFC) model, explicitly introduced to model elasticity in crystal growth [32–35]. In its basic formulation, the PFC model is based on a free energy analogous to the SH model, albeit with conservative dynamics  $\partial_t \psi = \nabla^2 (\delta F / \delta \psi)$ , where  $\psi$  can be considered as the time average of microscopic atomic density over vibrational timescales. The periodic patterns are then representative of lattices in crystalline materials. Such a model has been successfully applied to describe mesoscale phenomena in crystals, including elasticity effects during crystal growth, dislocation dynamics, and microstructure evolution [33, 35–38] also with non-conservative formulations which, *de facto*, correspond to the SH equation [39].

Elasticity is thus naturally encoded in SH/PFC models. By small perturbation of the periodicity of the order parameter, the energy can be written as a quadratic form of the strain [33, 40] resembling classical models of linear elasticity. Elastic constants are then related to the lattice symmetry described by  $\psi$ , and their magnitudes depend on the model parameters. Advanced models have also been proposed to account for elastic relaxation timescales [40–44]. Without approximations, the elastic energy that can be written upon displacing the density field also comprises higher-order terms, including nonlinear and strain-gradient terms. While the former have been the object of dedicated analyses [45–47], the latter have typically been neglected. However, numerical simulations exhibit features typical of GE. For instance, the stress field at dislocations in PFC simulations matches classical continuum elasticity in the far field but is nonsingular at their cores [47–50]. This is expected from a qualitative point of view as the fields  $\psi$  are smooth functions of spatial coordinates due to the underlying free energy functionals. However, the emerging regularization explicitly resembles that obtained in GE theories [20], for which preliminary evidence has been reported [47, 50]. In this work, we study how GE is encoded in SH and PFC models. The importance of establishing this connection is two-fold. On the one hand, related effects are present in numerical simulations. A comprehensive understanding of elasticity in the considered models allows for a better interpretation of simulation results and enables more rigorous applications to small-scale elasticity problems. On the other hand, the SH and PFC models provide microscopic theories for systems exhibiting order at a small scale, like reaction-diffusion systems and crystalline materials. As shown below, GE emerges naturally from the perturbation of their ground states. Therefore, GE is here self-consistently obtained as an elasticity theory valid at a small scale and connected to a prototypical, general framework for order-disorder phase transition.

This paper is organized as follows. In Sect. 2, we recall the basics of the GE theory, reporting the key information exploited in the current analysis. In Sect. 3, we first illustrate the SH free energy functional. Then we show how, in a simplified setting, GE naturally emerges from it upon perturbation of the microscopic density for both stripe (Sect. 4.1) and crystalline (Sect. 4.2) phases, also discussing extended parameterizations via the direct definition of a two-point correlation function (Sect. 4.3). In Sect. 5, we address in detail the effective GE theory that transpires without approximations in numerical simulations, focusing on the relevant case of the elastic field at dislocations. Therein, we also discuss the dependence of the characteristic lengths on model parameters and their implications. Conclusions are summarized in Sect. 6.

## 2. Gradient Elasticity

In *first strain-gradient elasticity* (GE-1), the elastic energy density accounts for strain and its first derivatives. In Toupin–Mindlin theory of anisotropic GE-1 [1, 2], it generally

reads ‡

$$w(\boldsymbol{\varepsilon}, \nabla \boldsymbol{\varepsilon}) = \frac{1}{2} \mathbb{C}_{ijkl} \varepsilon_{ij} \varepsilon_{kl} + \frac{1}{2} \mathbb{D}_{ijmkl n} \partial_m \varepsilon_{ij} \partial_n \varepsilon_{kl} + \mathbb{E}_{ijklm} \varepsilon_{ij} \partial_m \varepsilon_{kl}, \quad (1)$$

with  $\boldsymbol{\varepsilon} = \frac{1}{2}(\nabla \mathbf{u} + \nabla \mathbf{u}^\top)$  the strain tensor,  $\mathbf{u}$  the *macroscopic* displacement field, and  $\mathbb{C}$ ,  $\mathbb{E}$ , and  $\mathbb{D}$ , the constitutive four-, five- and six-rank tensors encoding elastic constants. This formulation simplifies the more general Mindlin's theory of elasticity in the presence of microstructures, which includes quantities at both macro and microscale [3, 5]. This multiscale formulation, however, can hardly be exploited for practical purposes, and gradient elasticity theories based on the macroscopic displacement  $\mathbf{u}$  are usually considered. In practice, the role played by microscopic deformation gradients is encoded by second gradients of the macroscopic displacement (Form I) or first gradients of the macroscopic strain (Form II), the latter leading to Eq. (1).  $\mathbb{C}$  and  $\mathbb{D}$  possess both minor and major symmetries, while  $\mathbb{E}$  has only minor symmetries. Illustrated for  $\mathbb{C}$ , these symmetries read component-wise

$$\mathbb{C}_{ijkl} = \mathbb{C}_{klij} \quad (\text{major}), \quad \mathbb{C}_{ijkl} = \mathbb{C}_{jikl} = \mathbb{C}_{ijlk} \quad (\text{minor}). \quad (2)$$

In the most general case, the constitutive tensors have 21, 108, and 171 independent components, respectively (in 3D), which may be derived from the energy density

$$\mathbb{C}_{ijkl} = \frac{\partial^2 w}{\partial \varepsilon_{ij} \partial \varepsilon_{kl}}, \quad \mathbb{E}_{ijklm} = \frac{\partial^2 w}{\partial \varepsilon_{ij} \partial (\partial_m \varepsilon_{kl})}, \quad \mathbb{D}_{ijmkl n} = \frac{\partial^2 w}{\partial (\partial_m \varepsilon_{ij}) \partial (\partial_n \varepsilon_{kl})}. \quad (3)$$

The quantities conjugate to the elastic strain and the gradient of the elastic strain are the Cauchy stress  $\boldsymbol{\sigma}$  and the double stress  $\boldsymbol{\tau}$

$$\sigma_{ij} = \frac{\partial w}{\partial \varepsilon_{ij}} = \mathbb{C}_{ijkl} \varepsilon_{kl} + \mathbb{E}_{ijklm} (\partial_m \varepsilon_{kl}), \quad (4)$$

$$\tau_{ijm} = \frac{\partial w}{\partial (\partial_m \varepsilon_{ij})} = \mathbb{E}_{klijm} (\partial_m \varepsilon_{kl}) + \mathbb{D}_{ijmkl n} (\partial_n \varepsilon_{kl}). \quad (5)$$

In isotropic and, more generally, centrosymmetric crystals,  $\mathbb{E}_{ijklm} = 0$ , resulting in the so-called Mindlin GE-1 for centrosymmetric material [3, 4]

$$w(\boldsymbol{\varepsilon}, \nabla \boldsymbol{\varepsilon}) = \frac{1}{2} \mathbb{C}_{ijkl} \varepsilon_{ij} \varepsilon_{kl} + \frac{1}{2} \mathbb{D}_{ijmkl n} \partial_m \varepsilon_{ij} \partial_n \varepsilon_{kl}. \quad (6)$$

The mechanical equilibrium condition (without body forces) reads

$$\partial_j (\sigma_{ij} - \partial_m \tau_{ijm}) = 0, \quad (7)$$

which can be recast in a field equation for the displacement:

$$\begin{aligned} L_{ik} u_k &= 0, \\ L_{ik} &= L_{ik}^{\mathbb{C}} - L_{ik}^{\mathbb{D}} = \mathbb{C}_{ijkl} \partial_j \partial_l - \mathbb{D}_{ijmkl n} \partial_j \partial_l \partial_m \partial_n. \end{aligned} \quad (8)$$

‡ we hereafter adopt Einstein summation convention

In the following, we will also use the Voigt notation for the fourth-order tensor  $\mathbb{C}$  using

$$11 \rightarrow 1, \quad 22 \rightarrow 2, \quad 33 \rightarrow 3, \quad 23 = 32 \rightarrow 4, \quad 13 = 31 \rightarrow 5, \quad 12 = 21 \rightarrow 6, \quad (9)$$

and for the six-order tensor  $\mathbb{D}$  using

$$\begin{aligned} 111 &\rightarrow 1, & 221 &\rightarrow 2, & 122 &\rightarrow 3, & 331 &\rightarrow 4, & 133 &\rightarrow 5, \\ 222 &\rightarrow 6, & 332 &\rightarrow 7, & 233 &\rightarrow 8, & 112 &\rightarrow 9, & 211 &\rightarrow 10, \\ 333 &\rightarrow 11, & 113 &\rightarrow 12, & 311 &\rightarrow 13, & 223 &\rightarrow 14, & 322 &\rightarrow 15, \\ 123 &\rightarrow 16, & 132 &\rightarrow 17, & 231 &\rightarrow 18. \end{aligned} \quad (10)$$

### 2.1. Isotropic materials

For isotropic materials,

$$\mathbb{C}_{ijkl} = \lambda \delta_{ij} \delta_{kl} + \mu (\delta_{ik} \delta_{jl} + \delta_{il} \delta_{jk}), \quad (11)$$

with  $\lambda$  and  $\mu$  the Lamé constants, and

$$\begin{aligned} \mathbb{D}_{ijmkl n} &= \frac{a_1}{2} (\delta_{ij} \delta_{km} \delta_{ln} + \delta_{ij} \delta_{kn} \delta_{lm} + \delta_{kl} \delta_{im} \delta_{jn} + \delta_{kl} \delta_{in} \delta_{jm}) + 2a_2 \delta_{ij} \delta_{kl} \delta_{mn} \\ &+ \frac{a_3}{2} (\delta_{jk} \delta_{im} \delta_{ln} + \delta_{ik} \delta_{jm} \delta_{ln} + \delta_{il} \delta_{jm} \delta_{kn} + \delta_{jl} \delta_{im} \delta_{kn}) + a_4 (\delta_{il} \delta_{jk} \delta_{mn} + \delta_{ik} \delta_{jl} \delta_{mn}) \\ &+ \frac{a_5}{2} (\delta_{jk} \delta_{in} \delta_{lm} + \delta_{ik} \delta_{jn} \delta_{lm} + \delta_{jl} \delta_{km} \delta_{in} + \delta_{il} \delta_{km} \delta_{jn}), \end{aligned} \quad (12)$$

with  $a_i$  coefficients of the strain-gradient terms. We thus obtain the elastic energy density

$$\begin{aligned} w_{\text{iso}} &= \frac{1}{2} \lambda \varepsilon_{ii} \varepsilon_{jj} + \mu \varepsilon_{ij} \varepsilon_{ij} + a_1 (\partial_j \varepsilon_{ii}) (\partial_k \varepsilon_{jk}) + a_2 (\partial_j \varepsilon_{ii}) (\partial_j \varepsilon_{kk}) \\ &+ a_3 (\partial_i \varepsilon_{ij}) (\partial_k \varepsilon_{jk}) + a_4 (\partial_k \varepsilon_{ij}) (\partial_k \varepsilon_{ij}) + a_5 (\partial_k \varepsilon_{ij}) (\partial_i \varepsilon_{jk}), \end{aligned} \quad (13)$$

and

$$L_{ik}^{\mathbb{C}} = (\lambda + 2\mu) \partial_i \partial_k + \mu (\delta_{ik} - \partial_i \partial_k), \quad (14)$$

$$L_{ik}^{\mathbb{D}} = 2(a_1 + a_2 + a_3 + a_4 + a_5) \partial_i \partial_k + \frac{1}{2} (a_3 + 2a_4 + a_5) (\delta_{ik} - \partial_i \partial_k). \quad (15)$$

One may redefine  $L_{ik}$  as

$$L_{ik} = (\lambda + 2\mu) [1 - \ell_1^2 \nabla^2] \partial_i \partial_k + \mu [1 - \ell_2^2 \nabla^2] (\delta_{ik} \nabla^2 - \partial_i \partial_k),$$

with  $\nabla^2$  the Laplacian and the two emerging *characteristic lengths*

$$\ell_1^2 = \frac{2(a_1 + a_2 + a_3 + a_4 + a_5)}{\lambda + 2\mu}, \quad (16)$$

$$\ell_2^2 = \frac{a_3 + 2a_4 + a_5}{2\mu}. \quad (17)$$

## 2.2. Centrosymmetric materials

For centrosymmetric materials,

$$\mathbb{C}_{ijkl} = C_{12}\delta_{ij}\delta_{kl} + C_{44}(\delta_{ik}\delta_{jl} + \delta_{il}\delta_{jk}) + (C_{11} - C_{12} - 2C_{44})\delta_{ijkl}, \quad (18)$$

with

$$\delta_{ijkl} = \begin{cases} 1, & \text{if } i = j = k = l, \\ 0, & \text{otherwise.} \end{cases} \quad (19)$$

The constants entering the prefactor of  $\delta_{ijkl}$  are typically used to quantify the anisotropy of a cubic material alternatively, e.g., via the so-called Zener ratio  $z = 2C_{44}/(C_{11} - C_{12})$  with  $z = 1$  for isotropic materials, for which Eq. (18) reduces to Eq. (11). The strain-gradient elasticity tensor can be written as

$$\begin{aligned} \mathbb{D}_{ijmkl n} = & \frac{a_1}{2}(\delta_{ij}\delta_{km}\delta_{ln} + \delta_{ij}\delta_{kn}\delta_{lm} + \delta_{kl}\delta_{im}\delta_{jn} + \delta_{kl}\delta_{in}\delta_{jm}) + 2a_2\delta_{ij}\delta_{kl}\delta_{mn} \\ & + \frac{a_3}{2}(\delta_{jk}\delta_{im}\delta_{ln} + \delta_{ik}\delta_{jm}\delta_{ln} + \delta_{il}\delta_{jm}\delta_{kn} + \delta_{jl}\delta_{im}\delta_{kn}) + a_4(\delta_{il}\delta_{jk}\delta_{mn} + \delta_{ik}\delta_{jl}\delta_{mn}) \\ & + \frac{a_5}{2}(\delta_{jk}\delta_{in}\delta_{lm} + \delta_{ik}\delta_{jn}\delta_{lm} + \delta_{jl}\delta_{km}\delta_{in} + \delta_{il}\delta_{km}\delta_{jn}) \\ & + a_6(\delta_{ik}\delta_{jlmn} + \delta_{il}\delta_{jkmn} + \delta_{jk}\delta_{ilmn} + \delta_{jl}\delta_{ikmn}) \\ & + a_7(\delta_{km}\delta_{ijln} + \delta_{lm}\delta_{ijkn} + \delta_{in}\delta_{jklm} + \delta_{jn}\delta_{iklm}) \\ & + a_8\delta_{mn}\delta_{ijkl} + a_9(\delta_{ij}\delta_{klmn} + \delta_{kl}\delta_{ijmn}) \\ & + a_{10}(\delta_{im}\delta_{jkl n} + \delta_{jm}\delta_{ikl n} + \delta_{kn}\delta_{ijl m} + \delta_{ln}\delta_{ijk m}) + a_{11}\delta_{ijklmn} \end{aligned} \quad (20)$$

Similarly to the case of isotropic material, one may define

$$\begin{aligned} \ell_1^2 &= \frac{2(a_1 + a_2 + a_3 + a_4 + a_5)}{C_{12} + 2C_{44}}, \\ \ell_2^2 &= \frac{a_3 + 2a_4 + a_5}{2C_{44}}, \\ \ell_3^2 &= \frac{a_6 + 2a_7 + a_8 + 2a_{10}}{C_{11} - C_{12} - 2C_{44}}, \end{aligned} \quad (21)$$

entering the operator  $L_{ik}$  for the generalized equations for displacements [21]:

$$\begin{aligned} L_{ik} = & (C_{11} + 2C_{44})[1 - \ell_1^2 \nabla^2] \partial_i \partial_k + C_{44}[1 - \ell_2^2 \nabla^2](\delta_{ik} \nabla^2 - \partial_i \partial_k) \\ & + (C_{11} - C_{12} - 2C_{44})[1 - \ell_3^2 \nabla^2] \delta_{ik} \partial_i \partial_k - (a_6 \delta_{ik} \delta_{jlmn} + a_{11} \delta_{ijklmn}) \partial_j \partial_l \partial_m \partial_n \\ & - (a_6 + a_7 + a_9 + a_{10})(\delta_{klmn} \partial_i + \delta_{ilmn} \partial_k) \partial_l \partial_m \partial_n. \end{aligned} \quad (22)$$

In this case, terms explicitly depending on  $a_i$  appear in  $L_{ik}$ , marking the inherent anisotropy of cubic crystals.

### 2.3. Special second-strain gradient elasticity

In *second strain-gradient elasticity* (GE-2), second derivatives of the strain field are retained in the elastic energy density,  $w \equiv w(\varepsilon_{ij}, \partial_k \varepsilon_{ij}, \partial_k \partial_\ell \varepsilon_{ij})$ . For isotropic materials, a special formulation can be considered still encoding two characteristic lengths  $\varrho_{1,2}$ . They enter the mechanical equilibrium condition as [21]

$$\begin{aligned} \partial_j [\sigma_{ij} - \partial_m \tau_{ijm} + \partial_n \partial_m \tau_{ijnm}] &= \partial_j [(1 - \varrho_1^2 \nabla^2)(1 - \varrho_2^2 \nabla^2) \sigma_{ij}] = 0 \\ &= \partial_j [(1 - \omega^2 \nabla^2 + \gamma^4 \nabla^4) \sigma_{ij}] = 0, \end{aligned} \quad (23)$$

with  $\tau_{ijnm} = \partial f / \partial (\partial_n \partial_m \varepsilon_{ij})$  the triple stress tensor and  $\nabla^4$  the bi-Laplacian. Constants relate as  $\omega^2 = \varrho_1^2 + \varrho_2^2$  and  $\gamma^4 = \varrho_1^2 \varrho_2^2$ . Note that to the leading order ( $\gamma = 0$ ), this theory reduces to a single characteristic length  $\omega$ , i.e. to GE-1 with  $\ell_1 = \ell_2 = \omega$ . This formulation has been exploited to obtain analytical solutions, e.g., for dislocation-induced deformations, which will be used in the following.

## 3. Swift-Hohenberg energy functional and elasticity

### 3.1. Free Energy for the microscopic density field

The Swift-Hohenberg (SH) and Phase-Field Crystal (PFC) model describe the non-conservative and conservative dynamics of a periodic order parameter  $\psi \equiv \psi(\mathbf{r})$ . The dynamical equation can be written in terms of the variation of a free energy functional  $F$  that, in its simplest form, can be written [27, 32]

$$F = \int_{\Omega} d\mathbf{x} \left[ \frac{1}{2} \psi \mathcal{L} \psi + \frac{1}{4} \psi^4 \right], \quad (24)$$

with  $\mathcal{L} = (q_0^2 + \nabla^2)^2 - \epsilon$ . This differential operator realizes an approximation of the first peak in the structure factor (at  $q_0$ ) of a periodic structure, namely a stripe or a crystalline phase. The so-called SH equation corresponds to the non-conservative  $L^2$ -gradient flow

$$\partial_t \psi = -\frac{\delta F}{\delta \psi} = [\epsilon - (q_0^2 + \nabla^2)^2] \psi - \psi^3. \quad (25)$$

The dynamics equation in the PFC model is instead given by the conservative  $H^{-1}$ -gradient flow

$$\partial_t \psi = \nabla^2 \frac{\delta F}{\delta \psi} = \nabla^2 \left\{ [(q_0^2 + \nabla^2)^2 - \epsilon] \psi + \psi^3 \right\}. \quad (26)$$

Eq. (24) realizes the minimal free energy to model order-disorder phase transition as its minimizing fields are either constant or periodic. As such, its form emerges in different contexts.  $F_\psi$  can be obtained as the non-dimensional form of the free energy describing liquid-solid transition with the order parameter corresponding to the microscopic density field  $\rho$  [33]

$$F_{\text{LS}} = \int_{\Omega} d\mathbf{r} \left[ \frac{1}{2} \rho \left( U \Delta T + \lambda (q_0^2 + \nabla^2)^2 \right) \rho + \frac{V}{4} \rho^4 \right], \quad (27)$$

with

$$\mathbf{r} = \mathbf{x}q_0, \quad \psi = \rho\sqrt{\frac{V}{\lambda q_0^4}}, \quad \epsilon = -\frac{U\Delta T}{\lambda q_0^4}, \quad F_\psi = \frac{F_{LS}}{F_0}, \quad F_0 = \frac{1}{V}\lambda^2 q_0^{8-d}, \quad (28)$$

$\Delta T = (T - T_s)/T_s$ , the relative temperature w.r.t the spinodal temperature  $T_s$ , and  $U$ ,  $V$ ,  $\lambda$  parameters. An SH energy functional for pure materials may also be derived—upon approximations—from the classical density functional theory [51–53] as discussed, e.g., in Refs. [34, 54–56]. One may consider the dimensionless deviation of the density  $\rho$  from its average  $\bar{\rho}$ ,  $n = (\rho - \bar{\rho})/\bar{\rho}$ , as order parameter. The local part, namely the nonlinear polynomial  $P(n)$  is then obtained as an approximation of the ideal-gas free energy, expanded as a power series up to the fourth order. The differential operator is obtained via the approximation of the  $n$ -point correlation  $C_n(\mathbf{r}_1, \mathbf{r}_2, \dots)$  in the excess energy term. The correlation function is truncated at  $C_2$  and approximated via an expansion up to the fourth order as  $C_2(|\mathbf{r} - \mathbf{r}'|) = (c_0 - c_2\nabla^2 + c_4\nabla^4)\delta(\mathbf{r} - \mathbf{r}')$ . The energy functional thus reads

$$\begin{aligned} F_c(\mathbf{r}) &= \int_{\Omega} d\mathbf{r} \left[ P(n(\mathbf{r})) - \frac{1}{2}n(\mathbf{r}) \int_{\Omega} C_2(|\mathbf{r} - \mathbf{r}'|)n(\mathbf{r}')d\mathbf{r}' \right] \\ &\approx \int_{\Omega} d\mathbf{r} \left[ P(n(\mathbf{r})) - \frac{1}{2}n(\mathbf{r})(c_0 - c_2\nabla^2 + c_4\nabla^4)n(\mathbf{r}) \right], \end{aligned} \quad (29)$$

and resembles Eq. (24) with, notably,  $R = \sqrt{2|c_4|/c_2} = 1/q_0$ . In the structural PFC model (XPFC) [57, 58], a more detailed control of the crystal structure is obtained by defining directly the correlation function in (29). Such a formulation is particularly well-suited for Fourier pseudo-spectral methods and  $C_2$  is typically defined via its Fourier transform  $\hat{C}_2(\mathbf{k})$ .

A multimode SH energy functional has also been proposed [59] with a differential operator approximating  $M$  peaks in the structure factor,

$$\mathcal{L}_M = \prod_{m=1}^M [(q_m^2 + \nabla^2)^2 + b_m], \quad (30)$$

where the  $b_m$  are additional constants controlling the stability of the corresponding modes. Without loss of generality, we consider here the multimode SH free-energy functional with the following generalized parameterization

$$F_\psi = \int_{\Omega} d\mathbf{x} \left[ A\psi\mathcal{L}_M\psi + B\psi^2 + C\psi^3 + D\psi^4 \right]. \quad (31)$$

### 3.2. Amplitude expansion

The density  $\psi$  can generally be expressed in terms of a small set of Fourier modes

$$\psi(\mathbf{r}) = \psi_0(\mathbf{r}) + \sum_{n=1}^N \eta_n(\mathbf{r})e^{i\mathbf{k}_n \cdot \mathbf{r}} + \text{c.c.}, \quad (32)$$



with  $\mathbf{k}_n$  the reciprocal space vectors and c.c. denoting the complex conjugate. For a relaxed crystal, amplitudes are real functions  $\eta_n = \varphi_n$  with  $\varphi_i = \varphi_j$  if  $|\mathbf{k}_i| = |\mathbf{k}_j|$ . A deformed crystal can be described by Eq. (32) with amplitudes being complex functions  $\eta_n(\mathbf{r}) = \varphi_n(\mathbf{r})e^{-i\mathbf{k}_n \cdot \mathbf{u}(\mathbf{r})}$  [45, 60, 61]. These complex amplitudes allow for the separation of different physical features [40]. For small deformations, the phase  $\theta_n = -\mathbf{k}_n \cdot \mathbf{u}$  encodes the deformation field, while  $\varphi_n(\mathbf{r})$  accounts for diffusive phenomena, melting or solidification (e.g., a transition from finite  $\varphi_n(\mathbf{r})$  to  $\varphi_n(\mathbf{r}) = 0$  would be representative of an order-disorder / solid-liquid interface).

In the amplitude expansion of the PFC model (APFC) [47], a free energy  $F_\eta$  dependent on amplitudes can be derived from  $F_\psi$ . For a one-mode approximation of  $\psi$  ( $M = 1$ ), this has been obtained via a renormalization group approach or by substituting (32) into the expression of the free energy functional and integrating over the unit cell [62–64]. Here, with the shortest reciprocal-space vector set to  $|\mathbf{k}_n| = q_0 = 1$  and focusing on bulk systems where  $\psi_0(\mathbf{r})$  can be assumed constant ( $\psi_0(\mathbf{r}) = \bar{\psi}$ ), we consider the amplitude approximation of the multimode SH functional (27) introduced in [65]

$$F_\eta = \int_{\Omega} d\mathbf{r} \left[ \sum_{n=1}^N (A' \Gamma_n |\mathcal{G}_n \eta_n|^2) + g^s(\{\eta_n\}) \right], \quad (33)$$

with  $\mathcal{G}_n = \nabla^2 + 2i\mathbf{k}_n \cdot \nabla$ ,  $g^s = \frac{B'}{2}\zeta_2 + \frac{C'}{3}\zeta_3 + \frac{D'}{4}\zeta_4 + E'$ ,  $\zeta_p$  complex polynomials of order  $p$  in the amplitudes depending on the lattice symmetry [47], and

$$\Gamma_n = \frac{\prod_{q_m \neq |\mathbf{k}_n|} [(q_m^2 - |\mathbf{k}_n|^2)^2 + b_m]}{\prod_{q_m \neq q_0} [(q_m^2 - q_0^2)^2 + b_m]} \quad (34)$$

where the denominator is chosen to enforce  $\Gamma_n = 1$  for the first mode. Parameters of (33) relate to the ones entering (31) as  $A' = A$ ,  $B' = B + 2C\bar{\psi} + 3D\bar{\psi}^2$ ,  $C' = C + 3D\bar{\psi}$ ,  $D' = D$ , and  $E' = (A/2)\bar{\psi}^2 + (C/3)\bar{\psi}^3 + (D/4)\bar{\psi}^4$ . The dynamic equation for amplitudes approximating Eq. (26) is

$$\partial_t \eta_n = -|\mathbf{k}_n|^2 \frac{\delta F_\eta}{\delta \eta_n^*}. \quad (35)$$

### 3.3. Elastic energy with strain gradient terms

As the displacement field varies over large length scales, elasticity in the SH or PFC model can be described by looking at amplitudes ( $\{\eta_j\}$ ) [40, 47]. In this context, the elastic energy density, namely the part of the energy depending on the displacement  $\mathbf{u}$  is

$$\mathcal{E} = \int_{\Omega} w(\{\eta_n\}) d\mathbf{x} = \int_{\Omega} \sum_n A \Gamma_n |\mathcal{G}_n \eta_n|^2 d\mathbf{x}. \quad (36)$$

Under the simplifying assumption of constant amplitude moduli ( $|\nabla\varphi_n| = 0$ ),

$$\begin{aligned}
|\mathcal{G}_n\eta_n|^2 = & 4\varphi_n^2(\mathbf{k}_n)_i(\mathbf{k}_n)_j(\mathbf{k}_n)_k(\mathbf{k}_n)_\ell \times \\
& \underbrace{\left[ (\partial_i u_j)(\partial_k u_\ell) - (\partial_i u_j)(\partial_k u_r)(\partial_\ell u_r) + \frac{1}{4}(\partial_i u_r)(\partial_j u_r)(\partial_k u_s)(\partial_\ell u_s) \right]}_{\mathbf{U}^2} \\
& + \varphi_n^2(\mathbf{k}_n)_i(\mathbf{k}_n)_j \underbrace{(\partial_{rr} u_i)(\partial_{ss} u_j)}_{\mathbf{G}^2},
\end{aligned} \tag{37}$$

with  $\mathbf{U}$  a non-linear strain tensor and  $\mathbf{G}$  encoding *gradient elasticity* contributions. Then, neglecting higher-order nonlinear terms, we have

$$w = A' \sum_n^N \Gamma_n \varphi_n^2 \left\{ 4[(\mathbf{k}_n)_i(\mathbf{k}_n)_j(\partial_i u_j)]^2 + [(\mathbf{k}_n)_i \nabla^2 u_i]^2 \right\}, \tag{38}$$

with the first and second terms in the sum corresponding to linear and strain-gradient elasticity terms, respectively. The latter may be rewritten as

$$A' \sum_{n=1}^N \Gamma_n \varphi_n^2 [(\mathbf{k}_n)_i \nabla^2 u_i]^2 = K \sum_i (\nabla^2 u_i)^2, \tag{39}$$

given that, for each mode (i.e., for each family of equal-length  $\mathbf{k}$ ), it holds true that

$$\sum_n (\mathbf{k}_n)_i^2 = Q, \quad \text{and} \quad \sum_n (\mathbf{k}_n)_i(\mathbf{k}_n)_j = 0, \quad \forall i \neq j, \tag{40}$$

where  $K$  and  $Q$  depend on the specific lattice symmetry and the number of modes considered.

To determine gradient-elasticity constants and characteristic lengths we then need to express the quantity (39) in terms of strain components. We consider 2D systems for brevity and without loss of generality. We have that

$$\begin{aligned}
(\nabla^2 u_x)^2 + (\nabla^2 u_y)^2 = & (\partial_x \varepsilon_{xx} + \partial_{yy}^2 u_x)^2 + (\partial_y \varepsilon_{yy} + \partial_{xx}^2 u_y)^2 \\
= & [(\partial_x \varepsilon_{xx})^2 + (\partial_y \varepsilon_{yy})^2] + 4[\partial_y \varepsilon_{xy} \partial_x \varepsilon_{xx} + \partial_x \varepsilon_{xy} \partial_y \varepsilon_{yy}] \\
& - 2[\partial_x \varepsilon_{yy} \partial_x \varepsilon_{xx} + \partial_y \varepsilon_{xx} \partial_y \varepsilon_{yy}] + [(\partial_x \varepsilon_{yy})^2 + (\partial_y \varepsilon_{xx})^2] \\
& + 4[(\partial_x \varepsilon_{xy})^2 + (\partial_y \varepsilon_{xy})^2] - 4[\partial_y \varepsilon_{xy} \partial_x \varepsilon_{yy} + \partial_x \varepsilon_{xy} \partial_y \varepsilon_{xx}],
\end{aligned} \tag{41}$$

where we exploited the identity  $\partial_{ii}^2 u_j = \partial_i(2\varepsilon_{ij} - \partial_j u_i) = 2\partial_i \varepsilon_{ij} - \partial_j \varepsilon_{ii}$ . This functional form for the elastic energy density matches the strain-gradient formulation for isotropic media. We may then compare terms of  $w$  to the general form of the elastic energy for isotropic materials (12):

$$\left\{ \begin{array}{ll} a_1 + a_2 + a_3 + a_4 + a_5 = K & \text{from } (\partial_x \varepsilon_{xx})^2, \\ a_1 + 2a_3 = 4K & \text{from } (\partial_y \varepsilon_{xy} \partial_x \varepsilon_{xx} + \partial_x \varepsilon_{xy} \partial_y \varepsilon_{yy}), \\ a_1 + 2a_2 = -2K & \text{from } (\partial_x \varepsilon_{yy} \partial_x \varepsilon_{xx} + \partial_y \varepsilon_{xx} \partial_y \varepsilon_{yy}), \\ a_2 + a_4 = K & \text{from } (\partial_x \varepsilon_{yy})^2 + (\partial_y \varepsilon_{xx})^2, \\ a_3 + 2a_4 + a_5 = 4K & \text{from } (\partial_x \varepsilon_{xy})^2 + (\partial_y \varepsilon_{xy})^2, \\ a_1 + 2a_5 = -4K & \text{from } (\partial_x \varepsilon_{yy} \partial_y \varepsilon_{xy} + \partial_y \varepsilon_{xx} \partial_x \varepsilon_{xy}), \end{array} \right. \tag{42}$$

By solving this system of (dependent) equations for  $a_i$  we obtain

$$2a_2 = -2K - a_1, \quad 2a_3 = 4K - a_1, \quad 2a_4 = K + a_1, \quad 2a_5 = -4K - a_1. \quad (43)$$

For three-dimensional systems, the expressions of coefficient  $a_i$  are analogous. This follows by considering the additional term  $(\nabla^2 u_z)^2$  on the left-hand side of Eq. (41) and proper extension of the right-hand side. The material length scales, as can be directly deduced from the first and fifth equations in (42), are

$$\ell_1 = \sqrt{\frac{2K}{\lambda + 2\mu}}, \quad \ell_2 = \sqrt{\frac{2K}{\mu}}, \quad (44)$$

with  $\ell_3 = 0$ . As a result, under the assumptions considered in this section, we establish that the SH energy functional encodes isotropic GE-1. We note that while no centrosymmetric crystal can verify the conditions for isotropic strain-gradient elasticity (due to the Hermann theorem [66]), for cubic materials that are nearly isotropic with respect to the constitutive four-rank tensor  $\mathbb{C}$ , a Voigt-type averaging procedure may be employed for the sixth-rank constitutive tensor  $\mathbb{D}$  in order to compute effective isotropic gradient-elastic constants [67]. In the following, we look at the expressions of the elastic energy density obtained for specific lattice symmetries.

## 4. Elastic constants and characteristic lengths from the SH functional

### 4.1. Stripe Phase

Stripe arrangements, e.g., in smectic phases [68–71] are a class of patterns described by SH and PFC models [27, 32]. The corresponding minimizer of the SH energy functional is well represented by waves with a single reciprocal lattice vector  $\mathbf{k}$ , namely with  $\psi$  described as in Eq. (32) with a single term in the sum. Assuming an arbitrarily oriented wave vector  $\mathbf{k} = k_0(\cos(\phi), \sin(\phi))$ , Eq. (38) reduces to:

$$\begin{aligned} \frac{w_{\text{str}}}{K_{\text{str}}} = & 4k_0^2(\cos^4(\phi)\varepsilon_{xx}^2 + \sin^4(\phi)\varepsilon_{yy}^2 + 2\cos^2(\phi)\sin^2(\phi)\varepsilon_{xx}\varepsilon_{yy} + 4\cos^2(\phi)\sin^2(\phi)\varepsilon_{xy}^2) \\ & + (\cos(\phi)\nabla^2 u_x + \sin(\phi)\nabla^2 u_y)^2, \end{aligned} \quad (45)$$

with  $K_{\text{str}} = A'\varphi^2 k_0^2$ . This leads to anisotropic elastic constants

$$\mathbb{C} = 8A'\varphi^2 k_0^4 \begin{pmatrix} \cos^4(\phi) & \cos^2(\phi)\sin^2(\phi) & \cos^3(\phi)\sin(\phi) \\ * & \sin^4(\phi) & \cos(\phi)\sin^3(\phi) \\ * & * & \cos^2(\phi)\sin^2(\phi) \end{pmatrix}. \quad (46)$$

Due to major and minor symmetries, there are 21 independent strain-gradient constants in 2D, reading (with  $k_0 = 1$ )

$$\begin{aligned} 2 \cos^2(\phi) &= D_{1,1} = D_{1,3} = D_{2,2} = D_{3,3} = -D_{1,2} = -D_{2,3}, \\ 2 \sin^2(\phi) &= D_{6,6} = D_{9,9} = D_{10,10} = D_{6,10} = -D_{6,9} = -D_{9,10}, \\ 2 \cos(\phi) \sin(\phi) &= D_{1,6} = D_{1,10} = D_{2,9} = D_{3,6} = D_{3,10} \\ &= -D_{1,9} = -D_{3,9} = -D_{2,6} = -D_{2,10}, \end{aligned} \quad (47)$$

Notice that in this case, the condition (39) is not met, and strain-gradient constants cannot be simply recast in the characteristic lengths  $\ell_i$ .

#### 4.2. Crystalline phases

The analysis of the density  $\psi$  for crystalline phases in SH and PFC models, e.g., to determine phase diagrams and elastic constants, is typically carried out by looking at the smallest number of modes in Eq. (32) required to describe a given lattice symmetry. In the coarse-grained APFC model, the number of modes enter the definition of the variables ( $\eta_n$ ) and thus leads to different solutions, i.e., different reconstructed  $\psi$  via Eq. (32). We consider here different crystalline phases: triangular, square, bcc, and fcc. For some representative cases, we analyze different numbers of modes. We report the elastic energy density for the different symmetries/approximations, set by specific choices for  $\mathbf{k}_n$  with  $\min_{n=1}^N |\mathbf{k}_n| = 1$  (without loss of generality considering adimensional spatial lengths  $\mathbf{x} = \mathbf{r}R^{-1} = \mathbf{r}q_0$ ), the corresponding elastic constants, and GE characteristic lengths for small deformations and neglecting nonlinearities (see Table 1 and Fig. 2). We introduce the scaling factor  $k_0$  such that  $a_0 = 2\pi/k_0$  is the interatomic distance.

*Triangular phase, one-mode approximation (tri-1):*

$$\mathbf{k}_1 = k_0(-1, -1/\sqrt{3}), \quad \mathbf{k}_2 = k_0(0, 2/\sqrt{3}), \quad \mathbf{k}_3 = k_0(1, -1/\sqrt{3}).$$

with  $k_0 = \sqrt{3}/2$ . Elastic energy density:

$$\frac{w_{\text{tri-1}}}{K_{\text{tri-1}}} = 4k_0^2(\varepsilon_{xx}^2 + \varepsilon_{yy}^2) + \frac{8}{3}k_0^2\varepsilon_{xx}\varepsilon_{yy} + \frac{16}{3}k_0^2\varepsilon_{xy}^2 + (\nabla^2 u_x)^2 + (\nabla^2 u_y)^2, \quad (48)$$

with  $K_{\text{tri-1}} = 2A'\varphi_1^2 k_0^2$ .

*Triangular phase, two-mode approximation (tri-2):*

$$\begin{aligned} \mathbf{k}_1 &= k_0(-1, -1/\sqrt{3}), & \mathbf{k}_2 &= k_0(0, 2/\sqrt{3}), & \mathbf{k}_3 &= k_0(1, -1/\sqrt{3}), \\ \mathbf{k}_4 &= k_0(-1, -\sqrt{3}), & \mathbf{k}_5 &= k_0(-1, \sqrt{3}), & \mathbf{k}_6 &= k_0(2, 0), \end{aligned}$$

with  $k_0 = \sqrt{3}/2$ . Elastic energy density:

$$\frac{w_{\text{tri-2}}}{K_{\text{tri-2}}} = 4\alpha^2 k_0^2(\varepsilon_{xx}^2 + \varepsilon_{yy}^2) + \frac{8}{3}\alpha^2 k_0^2\varepsilon_{xx}\varepsilon_{yy} + \frac{16}{3}\alpha^2 k_0^2\varepsilon_{xy}^2 + (\nabla^2 u_x)^2 + (\nabla^2 u_y)^2, \quad (49)$$

with  $K_{\text{tri-2}} = 2A'(\varphi_1^2 + 3\varphi_2^2)k_0^2$  and  $\alpha^2 = (\varphi_1^2 + 9\varphi_2^2)/(\varphi_1^2 + 3\varphi_2^2)$ .

*Square lattice, two-mode approximation (sq-2):*

$$\mathbf{k}_1 = k_0(1, 0), \quad \mathbf{k}_2 = k_0(0, 1), \quad \mathbf{k}_3 = k_0(1, 1), \quad \mathbf{k}_4 = k_0(1, -1),$$

with  $k_0 = 1$ . Elastic energy density:

$$\frac{w_{\text{sq-2}}}{K_{\text{sq-2}}} = 4k_0^2(\varepsilon_{xx}^2 + \varepsilon_{yy}^2) + 16\alpha^2 k_0^2 \varepsilon_{xx} \varepsilon_{yy} + 32\alpha^2 k_0^2 \varepsilon_{xy}^2 + (\nabla^2 u_x)^2 + (\nabla^2 u_y)^2, \quad (50)$$

with  $K_{\text{sq-2}} = A'(\varphi_1^2 + 2\varphi_2^2)k_0^2$  and  $\alpha^2 = \varphi_2^2/(\varphi_1^2 + 2\varphi_2^2)$ .

*BCC lattice, one-mode approximation (bcc-1):*

$$\begin{aligned} \mathbf{k}_1 &= k_0\sqrt{3}/2(0, 1, 1), & \mathbf{k}_2 &= k_0\sqrt{3}/2(1, 0, 1), & \mathbf{k}_3 &= k_0\sqrt{3}/2(1, 1, 0), \\ \mathbf{k}_4 &= k_0\sqrt{3}/2(0, 1, -1), & \mathbf{k}_5 &= k_0\sqrt{3}/2(1, -1, 0), & \mathbf{k}_6 &= k_0\sqrt{3}/2(-1, 0, 1), \end{aligned}$$

with  $k_0 = \sqrt{2/3}$ . Elastic energy density:

$$\begin{aligned} \frac{w_{\text{bcc-1}}}{K_{\text{bcc-1}}} &= 3k_0^2(\varepsilon_{xx}^2 + \varepsilon_{yy}^2 + \varepsilon_{zz}^2) + 3k_0^2(\varepsilon_{xx}\varepsilon_{yy} + \varepsilon_{xx}\varepsilon_{zz} + \varepsilon_{yy}\varepsilon_{zz}) \\ &\quad + 6k_0^2(\varepsilon_{xy}^2 + \varepsilon_{xz}^2 + \varepsilon_{yz}^2) + (\nabla^2 u_x)^2 + (\nabla^2 u_y)^2 + (\nabla^2 u_z)^2, \end{aligned} \quad (51)$$

with  $K_{\text{bcc-1}} = 3A'k_0^2\varphi_1^2$ .

*BCC lattice, two-mode approximation (bcc-2):*

$$\begin{aligned} \mathbf{k}_1 &= k_0\sqrt{3}/2(0, 1, 1), & \mathbf{k}_2 &= k_0\sqrt{3}/2(1, 0, 1), & \mathbf{k}_3 &= k_0\sqrt{3}/2(1, 1, 0), \\ \mathbf{k}_4 &= k_0\sqrt{3}/2(0, 1, -1), & \mathbf{k}_5 &= k_0\sqrt{3}/2(1, -1, 0), & \mathbf{k}_6 &= k_0\sqrt{3}/2(-1, 0, 1), \\ \mathbf{k}_7 &= k_0\sqrt{3}(1, 0, 0), & \mathbf{k}_8 &= k_0\sqrt{3}(0, 1, 0), & \mathbf{k}_9 &= k_0\sqrt{3}(0, 0, 1), \end{aligned}$$

with  $k_0 = \sqrt{2/3}$ . Elastic energy density:

$$\begin{aligned} \frac{w_{\text{bcc-2}}}{K_{\text{bcc-2}}} &= 3\frac{\varphi_1^2 + 4\varphi_2^2}{\varphi_1^2 + \varphi_2^2}k_0^2(\varepsilon_{xx}^2 + \varepsilon_{yy}^2 + \varepsilon_{zz}^2) + 3\alpha^2 k_0^2(\varepsilon_{xx}\varepsilon_{yy} + \varepsilon_{xx}\varepsilon_{zz} + \varepsilon_{yy}\varepsilon_{zz}) \\ &\quad + 6\alpha^2 k_0^2(\varepsilon_{xy}^2 + \varepsilon_{xz}^2 + \varepsilon_{yz}^2) + (\nabla^2 u_x)^2 + (\nabla^2 u_y)^2 + (\nabla^2 u_z)^2, \end{aligned} \quad (52)$$

with  $K_{\text{bcc-2}} = 3A'k_0^2(\varphi_1^2 + \varphi_2^2)$  and  $\alpha^2 = \varphi_1^2/(\varphi_1^2 + \varphi_2^2)$ .

*FCC lattice, two-mode approximation (fcc-2):*

$$\begin{aligned} \mathbf{k}_1 &= k_0/\sqrt{2}(-1, 1, 1), & \mathbf{k}_2 &= k_0/\sqrt{2}(1, -1, 1), \\ \mathbf{k}_3 &= k_0/\sqrt{2}(1, 1, -1), & \mathbf{k}_4 &= k_0/\sqrt{2}(-1, -1, -1), \\ \mathbf{k}_5 &= k_0\sqrt{2}(1, 0, 0), & \mathbf{k}_6 &= k_0\sqrt{2}(0, 1, 0), & \mathbf{k}_7 &= k_0\sqrt{2}(0, 0, 1), \end{aligned}$$

with  $k_0 = \sqrt{2/3}$ . Elastic energy density:

$$\begin{aligned} \frac{w_{\text{fcc-2}}}{K_{\text{fcc-2}}} = & 2 \frac{\varphi_1^2 + 4\varphi_2^2}{\varphi_1^2 + \varphi_2^2} k_0^2 (\varepsilon_{xx}^2 + \varepsilon_{yy}^2 + \varepsilon_{zz}^2) + 4\alpha^2 k_0^2 (\varepsilon_{xx}\varepsilon_{yy} + \varepsilon_{xx}\varepsilon_{zz} + \varepsilon_{yy}\varepsilon_{zz}) \\ & + 8\alpha^2 k_0^2 (\varepsilon_{xy}^2 + \varepsilon_{xz}^2 + \varepsilon_{yz}^2) + (\nabla^2 u_x)^2 + (\nabla^2 u_y)^2 + (\nabla^2 u_z)^2, \end{aligned} \quad (53)$$

with  $K_{\text{fcc-2}} = 2A'k_0^2(\varphi_1^2 + \varphi_2^2)$  and  $\alpha^2 = \varphi_1^2/(\varphi_1^2 + \varphi_2^2)$ .

The elastic constants and GE characteristic lengths obtained via Eq. (21) from the elastic energy densities above are reported in Table 1. Note that for all lattice symmetries, the constraint  $C_{12} = C_{44}$  holds. Interestingly, this corresponds to the Cauchy relation derived in the lattice-theoretical description of constitutive tensors for central force interaction between atoms [67, 72].

Symmetry	$C_{11}$ ( $A'k_0^4$ )	$C_{12} = C_{44}$ ( $A'k_0^4$ )	$\ell_1$ ( $a_0$ )	$\ell_2$ ( $a_0$ )	$\alpha^2$
tri-1	$16\varphi_1^2$	$\frac{16}{3}\varphi_1^2$	$\frac{1}{4\pi}$	$\frac{\sqrt{3}}{4\pi}$	—
tri-2	$16(\varphi_1^2 + 9\varphi_2^2)$	$\frac{16}{3}(\varphi_1^2 + 9\varphi_2^2)$	$\frac{1}{4\pi} \frac{1}{\alpha}$	$\frac{\sqrt{3}}{4\pi} \frac{1}{\alpha}$	$\frac{\varphi_1^2 + 9\varphi_2^2}{\varphi_1^2 + 3\varphi_2^2}$
sq-2	$8(\varphi_1^2 + 2\varphi_2^2)$	$16\varphi_2^2$	$\frac{1}{4\pi\sqrt{6}} \frac{1}{\alpha}$	$\frac{1}{4\pi\sqrt{2}} \frac{1}{\alpha}$	$\frac{\varphi_2^2}{\varphi_1^2 + 2\varphi_2^2}$
bcc-1	$18\varphi_1^2$	$9\varphi_1^2$	$\frac{1}{3\pi\sqrt{2}}$	$\frac{1}{\pi\sqrt{6}}$	—
bcc-2	$18(\varphi_1^2 + 4\varphi_2^2)$	$9\varphi_1^2$	$\frac{1}{3\pi\sqrt{2}} \frac{1}{\alpha}$	$\frac{1}{\pi\sqrt{6}} \frac{1}{\alpha}$	$\frac{\varphi_1^2}{\varphi_1^2 + \varphi_2^2}$
fcc-2	$8(\varphi_1^2 + 4\varphi_2^2)$	$8\varphi_1^2$	$\frac{1}{2\pi\sqrt{6}} \frac{1}{\alpha}$	$\frac{1}{2\pi\sqrt{2}} \frac{1}{\alpha}$	$\frac{\varphi_1^2}{\varphi_1^2 + \varphi_2^2}$

**Table 1.** Elastic constants and characteristic lengths for the different lattice symmetries and approximations of the microscopic density with a different number of modes for triangular and bcc lattices.

We find that  $\ell_2/\ell_1 = \sqrt{3}$ , as a result of the general form of the (isotropic) strain-gradient terms reported in Sect. 3.3. Typical values found or adopted in the literature for this ratio are close to one [73, 74]. For a one-mode approximation of  $\psi$  (one length of  $\mathbf{k}$  considered), length scales are constants. For approximations of  $\psi$  considering more than one mode, characteristic lengths depend on  $\varphi_i$ . Figure 1 illustrates the bulk free energy density for the *tri-2* (Fig. 1a) and *fcc-2* (Fig. 1b) case as a function of  $\varphi_1$  and  $\varphi_2$  for selected parameters. The global minima of these free energy densities (blue squares) correspond to the equilibrium phase. Values of  $\varphi_1$  and  $\varphi_2$  vary with the free energy parameters as dictated by the energy landscape so they are not free parameters entering  $\alpha$ . An illustration of their variation is reported in Fig. 1c (*tri-2*) and 1d (*fcc-2*).

Figure 2 reports the values of  $\ell_{1,2}$  by varying  $B$  in the free energy for a selected parameter range where all the symmetries can be explored for  $B < B_c$  and  $B_c$  corresponding to the order-disorder critical point [47]. Here the effect of changes in  $\varphi_i$  is then quantified for a specific choice of parameters. We note that a limited change is

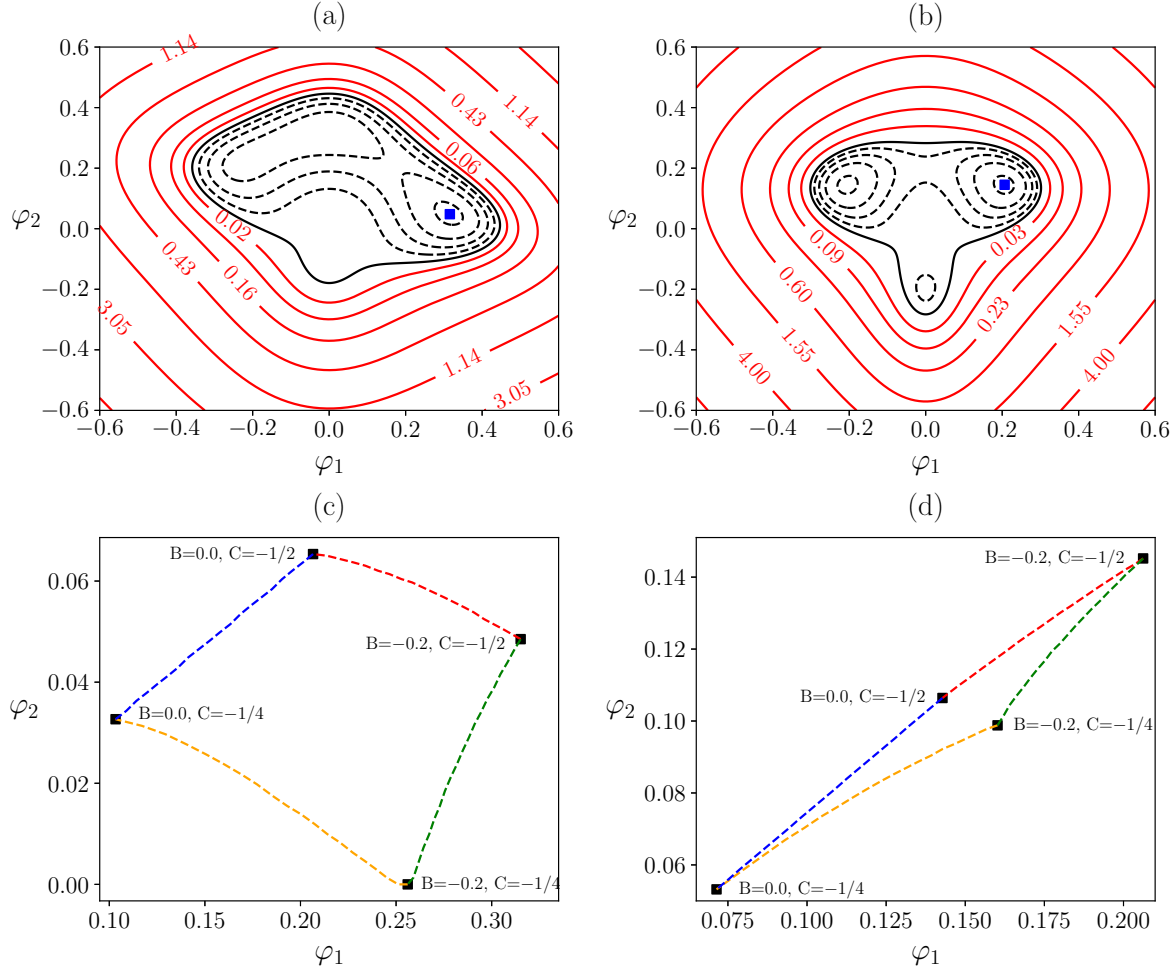


**Figure 1.** Bulk free energy density  $f(\varphi_1, \varphi_2)$  for (a) triangular (2 modes) and (b) fcc (2 modes) for  $B = -0.2$ ,  $C = -1/2$ , and  $D = 1/3$ . Solid red lines and dashed black lines are positive and negative values, respectively (values on contour lines are multiplied by  $10^2$ ). The blue square indicates the global minimum. The variation of the amplitudes  $\varphi_{1,2}$  minimizing the energy by varying parameters  $B$  and  $C$  (with  $D = 1/3$ ) is also illustrated for (c) triangular (2 modes) and (d) fcc (2 modes). Four representative configurations are illustrated (black squares). Dashed lines are obtained by varying the parameter that changes in the squares they connect.

observed among all the explored ranges ( $\lesssim 10\%$ ). The lattice symmetry is found to affect the values of the GE length scales. At small enough  $B$ , the number of modes considered does not impact the characteristic lengths whereas a clear deviation is observed at larger  $B$  (Fig. 2). In the context of APFC, these approximations realize different models as the choice of modes dictates the variables to solve for in the system (the amplitudes  $\eta_j$ ). Instead, for PFC and SH, considering a larger number of modes results in a better estimation of the model's elastic properties.

The values of  $\ell_{1,2}$  in Fig. 2 are reported in terms of the ratio with the spatial length scale entering the free energy, namely the lattice parameter  $a_0 = 2\pi/k_0$ , with  $k_0$  depending on the lattice symmetry (see specific values together with the definition

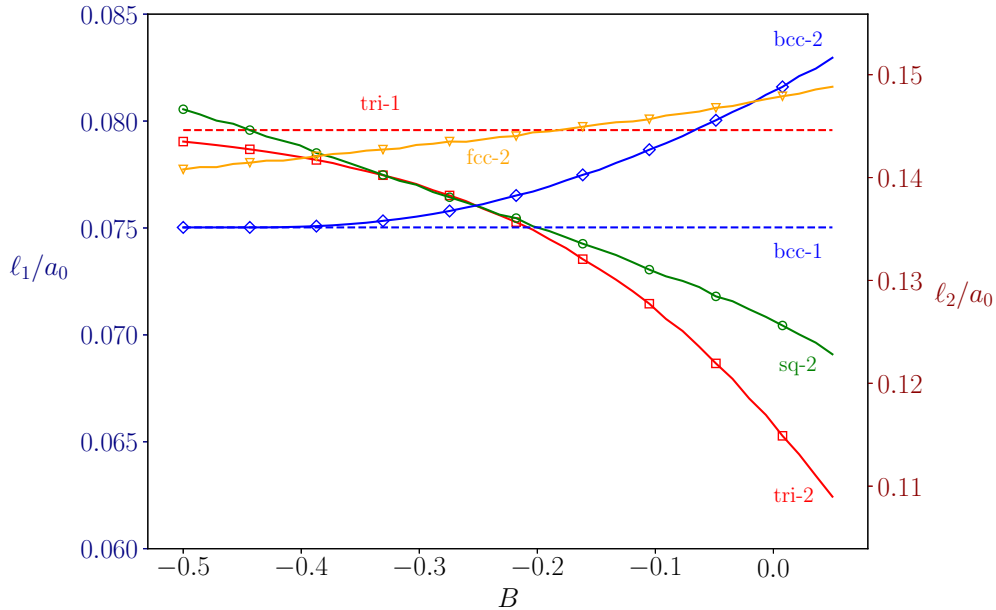


**Figure 2.** Characteristic lengths  $\ell_1$  and  $\ell_2$  by varying  $B$  with  $C = -1/2$  and  $D = 1/3$  as from Table 1. Dashed lines correspond to the length scales for one mode approximations, available for triangular and bcc symmetry only.

of reciprocal space vectors). They all correspond to fractions of the lattice spacing. Therefore they are in the order of  $\sim 10^{-10}\text{m}$  ( $\text{\AA}$ ) when looking at physical units of common materials, in line with GE literature [17, 74]. From a quantitative point of view, however, we note that the ratio of the GE length scales with the lattice parameters does not precisely match typical values computed with *ab initio* approaches [17]. As with the determination of elastic constants for the classical linear elasticity terms, the considered minimal models encode general features of GE while quantitative descriptions should be addressed by more advanced formulations [57, 75], outlined in the following section.

An important aspect emerging from this analysis is that the GE length scales, being of the order of  $1\text{\AA}$ , are typically smaller than the coarse-graining lengths that should be considered in PFC-like approaches to work with continuous elastic field (filtering out microscopic fluctuation) or underlying the derivation of the corresponding equations for APFC approaches. Therefore, while GE is self-consistently encoded, specific features emerging at those length scales are expected to be coarse-grained. This aspect is discussed further below with the aid of numerical examples.

#### 4.3. Characteristic lengths from structural PFC: triangular symmetry

Energy functionals generalizing Eq. (31), or Eq. (33) for amplitude formulations, can be devised by modeling the correlation function in Eq. (29) directly [57, 76]. Such an approach proved powerful in devising parametrization to model specific materials, e.g.,



in Ref. [75]. We outline here the possibility of devising a parametrization of GE length scales by designing the correlation function. For illustrative purposes, we focus here on the 1-mode triangular symmetry.

For a generic two-point correlation function  $C_2$ , the elastic energy takes the form:

$$\mathcal{F}_{\text{el}} = \mathcal{F}[\psi(\mathbf{r} + \mathbf{u}(\mathbf{r}))] - \mathcal{F}[\psi(\mathbf{r})], \quad (54)$$

where

$$\mathcal{F}[\psi(\mathbf{r})] = \int \psi(\mathbf{r}) \cdot (C_2 * \psi)(\mathbf{r}) \, d^2\mathbf{r}. \quad (55)$$

To allow for the analytical derivation of the elastic and gradient-elastic constants, we consider a polynomial expansion of  $C_2$  in the reciprocal space—corresponding to the Dirac delta function and its derivatives in real space—so that the convolution can be carried out explicitly, leading to differentiation of  $\mathbf{u}(\mathbf{r})$ . We consider a polynomial expansion of the Fourier transform of  $C_2$  reading

$$\widehat{C}_2(|\mathbf{k}|) = \sum_{n=0}^N c_{2n} |\mathbf{k}|^{2n}, \quad (56)$$

where we consider even terms only due to symmetry consideration, consistently with Eq. (29). For an  $N$ -term expansion, we then retain up to order  $2N$  with  $N$  coefficients.

Here we consider a setting that introduces additional parameters while reproducing the features of GE elasticity obtained by the minimal SH energy functional. Therefore we impose constraints on the form of  $\widehat{C}_2(|\mathbf{k}|)$  in order to fulfill the following requirements: i) peak in the correlation function at  $|\mathbf{k}| = 1$  (as above); ii) value of the peak set to 0 such to have the same phenomenological temperature ( $B$ , see also Sect. 3) as in the minimal models; iii) same elastic constants as the triangular 1-mode (see Table 1); iv) isotropic GE as obtained in Sect. 3.3. All these requirements are independent. Moreover, the last one enforcing isotropic GE imposes two constraints with a total of 5 conditions on coefficients in Eq. (56). Therefore, we need a minimum of  $N = 6$  to tune the characteristic lengths independently, yielding

$$c_2 = 2 - 3c_{12}, \quad c_4 = 1 - 9c_{12}, \quad c_6 = -8c_{12}, \quad c_8 = 0, \quad c_{10} = 3c_{12}. \quad (57)$$

This then results in the following length scales, now featuring a free parameter ( $c_{12}$ )

$$\ell_1^2 = \frac{1}{3} - 6c_{12}, \quad \ell_2^2 = 1 - 6c_{12}. \quad (58)$$

Note that the value, as well as the ratio between length scales, now depends on the free parameter. Finally, to ensure higher frequencies are suppressed relative to lower ones and real positive characteristic lengths,  $c_{12} \geq 0$  and  $c_{12} \leq 1/18$  must hold, respectively, thus implying  $\ell_1/\ell_2 \in [0, 1/\sqrt{3}]$ . In this setting, we then reproduced the model conveyed by the minimal SH energy functional, for both linear elasticity and GE, with an extended parameterization. Following similar procedures, we envisage that parametrized SH- or PFC-like models can be devised by considering appropriate expansions of  $C_2$  and constraints.

## 5. Effective GE length scales at dislocations

Coarse-graining should be considered in microscopic models to obtain the *macroscopic* displacement field  $\mathbf{u}$ , and thus deformation fields (see also Sect. 2). In PFC models, this coarse-graining length is in the order of the lattice parameter [47, 77], while characteristic GE lengths obtained above are significantly smaller. The interplay with the correlation length of phases  $W$ , a characteristic length incorporated in the SH energy corresponding to the distance over which the system properties are affected by the phase in a given position [78], is expected. This, for instance, recently emerged for the size of the dislocation core in the PFC model. Although they possess the same topological charge (the Burgers vector), dislocations exhibit a core size that scales with  $W$  to some extent [79].

Without approximations, linear, nonlinear, and gradient-elasticity contributions must be considered to fully characterize elasticity in the SH and PFC models. In addition, to accurately encode the dependence of physical constants on model parameters, advanced frameworks must be considered, including, e.g., the variation of amplitude magnitudes [45, 80, 81], assumed constants in the analysis of Sect. 3. These and related aspects prevent us from fully deriving analytic or semi-analytic expressions for GE constants, particularly in realistic settings featuring nonuniform strain variations and nontrivial solutions. However, with the aid of numerical simulations, we show here that the elasticity encoded in the considered models matches very well with known predictions from strain-gradient elasticity by using effective characteristic lengths. Moreover, it allows us to characterize additional effects and unveil their dependence on model parameters.

We look in particular at one of the key evidence concerning GE at the microscale, namely the regularization of the elastic field at dislocations [20], which is also of central interest for crystalline systems. We consider the APFC model for simplicity, encoding a natural coarse-graining length in the equation (the lattice parameter [47]). Accordingly, the elastic field can be directly computed from  $\eta_j$  rather than upon numerical coarse-graining (see also Eq. A.4).

An edge dislocation can be simulated by setting the complex amplitudes' phases as  $\theta_n = -\mathbf{k}_n \cdot \mathbf{u}^{\text{dislo}}$  [47] and letting the system evolve to equilibrium, with

$$\begin{aligned} u_x^{\text{dislo}} &= \frac{b}{2\pi} \left[ \arctan\left(\frac{y}{x}\right) + \frac{xy}{2(1-\nu)(x^2+y^2)} \right], \\ u_y^{\text{dislo}} &= -\frac{b}{2\pi} \left[ \frac{(1-2\nu)}{4(1-\nu)} \log(x^2+y^2) + \frac{x^2-y^2}{4(1-\nu)(x^2+y^2)} \right], \end{aligned} \quad (59)$$

the dislocation displacement field,  $\mathbf{b} = b_x \hat{\mathbf{x}}$  the Burgers vector, and  $\nu$  the Poisson's ratio [24]. In general, defect arrangements evolve dynamically [44]. To study elastic fields at defects, we consider a static configuration. It consists of a checkered pattern, nominally on a square grid, of dislocations having  $\pm \mathbf{b}$  as Burgers vectors and distance  $L/2$ . Notice, however, that due to the underlying triangular symmetry, dislocations

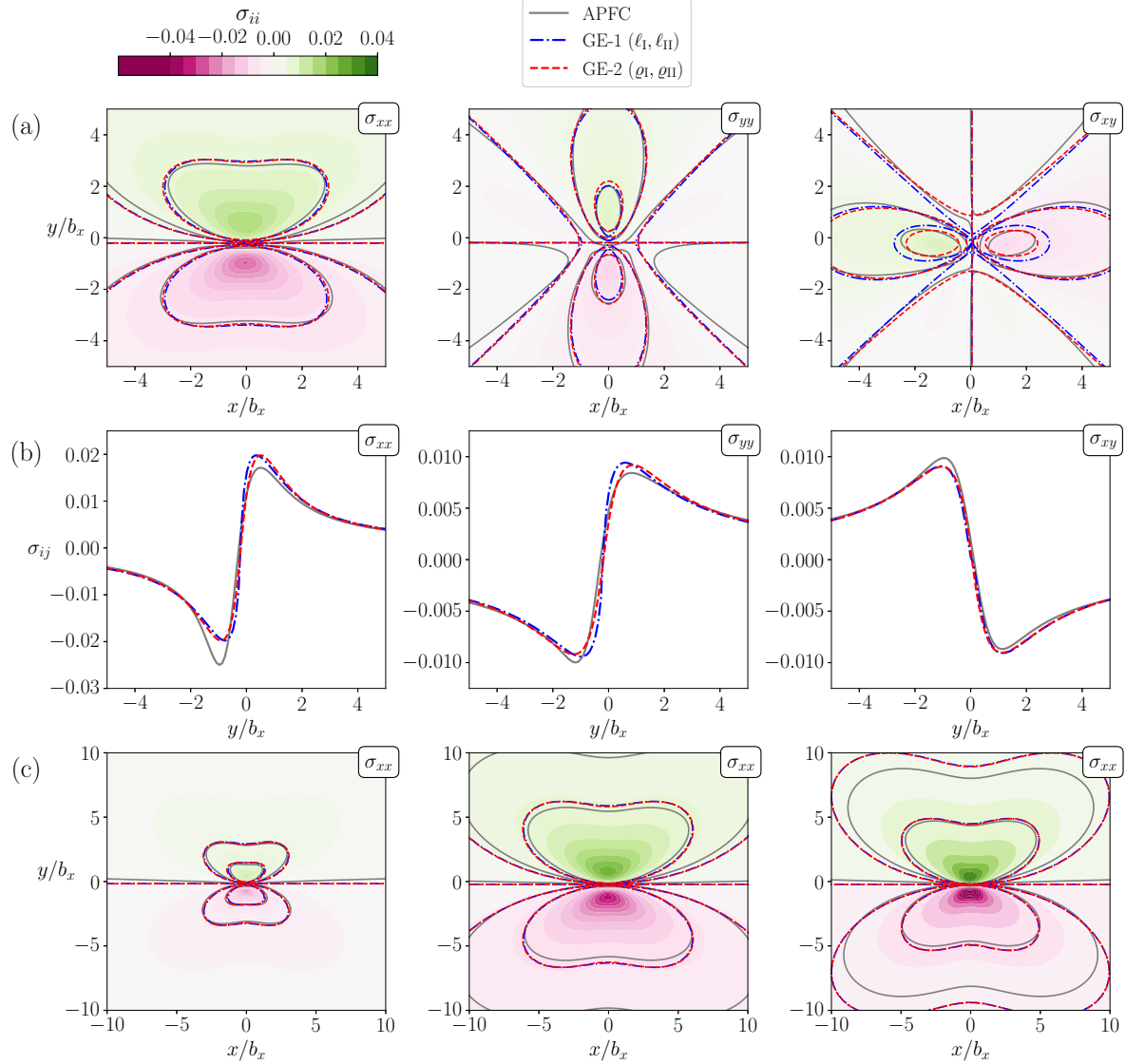


**Figure 3.** Stress field from APFC modeling of an edge dislocation in a triangular lattice (*tri-1*) compared to the predictions of GE-1 and GE-2 for an isotropic medium. Characteristic lengths,  $(\ell_I, \ell_{II})$  for GE-1 and  $(\varrho_I, \varrho_{II})$  for GE-2, are obtained by fitting Eqs. (B.1)–(B.3) and (B.4)–(B.6), respectively, to the APFC numerical result (see further details and values obtained by fitting in Appendix C). APFC results are shown with solid grey contour lines and the underlying colormap to note negative and positive stress regions. GE-1 with fitted length scales is illustrated via dot-dashed blue lines, and GE-2 via dashed red lines. Contour lines are set to the same values in all the 2D plots of the stress to  $[-7, -3.5, 0.0, 3.5, 7] \times 10^{-3}$ . The same applies to the range of color maps. (a) 2D contour plots of the stress field components  $\sigma_{xx}$ ,  $\sigma_{yy}$ , and  $\sigma_{xy}$  (from left to right) for  $A = 1$ ,  $B = 0.02$ . (b) Detailed comparison as 1D curves of the values in panel (a) along  $y$  at  $x = 0$  for  $\sigma_{xx}$  and  $\sigma_{yy}$ , and along  $x$  for  $\sigma_{xy}$  (from left to right). (c)  $\sigma_{xx}$  illustrated as in panel (a) for three different parameter choices. From left to right parameters  $(A, B)$  are set to:  $(0.5, 0.02)$ ,  $(2.0, 0.02)$  and  $(1, -0.026)$ . In all plots  $b_x = -a_0$ ,  $C = -1/2$ , and  $D = 1/3$ .

cannot be placed exactly on a square grid, and the relaxation of the initial condition leads to a small shift in their positions. However, this configuration allows simulating a static, periodic system by considering an  $L \times L$  box. We remark that the displacement field in Eqs. (59) is exact for an isotropic medium within linear elasticity [24]. Here, it is exploited to introduce dislocation with the desired Burgers vector. By letting the system relax to equilibrium, its adaptation to the actual solution, including the effects outlined in (37), is obtained. Analogous results, but with a slower convergence to the equilibrium solution, can be obtained by setting proper singularities in  $\theta_n$  without initial assumption on the elastic field as done, e.g., in Refs. [48]. Numerical results are obtained by exploiting a simple pseudo-spectral Fourier method as summarized in Appendix A.

Figure 3 illustrates the stress field of an edge dislocation in a triangular crystal as obtained at equilibrium by APFC simulations compared to the prediction of GE theories with fitted characteristic lengths. We consider solutions for an edge dislocation in an isotropic medium obtained within GE-1 and GE-2 as reported in Refs. [21] and [23], respectively. Corresponding equations are reported in Appendix B, while details of the fitting procedure are given in Appendix C (fitted values of the characteristic lengths  $\ell_i$  and  $\varrho_i$  are indicated with the subscripts “I” and “II” in the following). GE-1 is the theory emerging from the analysis reported in Sect. 3. GE-2 includes higher-order contributions. Importantly, the solution of the elastic field for a dislocation in GE-2 features smaller gradients (see Fig. B1) at the core, as further discussed below.

In particular, Fig. 3a shows stress field components in 2D for a selected set of parameters. Color maps and representative grey contour lines illustrate the value obtained by numerical APFC simulations. The stress field along lines crossing the dislocation core parallel to the  $y$ -axis for  $\sigma_{xx}$  and  $\sigma_{yy}$  and the  $x$ -axis for  $\sigma_{xy}$  are shown in Fig. 3b.  $\sigma_{ij}$  from APFC simulations are regularized at the core, and both GE-1 and GE-2 solutions match very well the results of numerical simulations for some values of the respective characteristic lengths ( $\ell_i$  and  $\varrho_i$ ). As observed in other works [47], the elastic field obtained by APFC is asymmetric, a feature that is absent in the considered GE theories as it results from nonlinearities in the free-energy functional [45]. Accordingly, this effect is more pronounced for larger stress values, namely for  $\sigma_{xx}$  where the stress field reaches maximum and minimum values two times larger than other components’. Length scales have been determined by fitting the numerically computed values for the stress components via the analytical solution for both GE-1 and GE-2 (reported in Appendix B). Characteristic lengths and dislocation positions (subject to the small shift mentioned above) are retained as fitting parameters. Their values, determined via the fitting performed to obtain the plots in Fig. 3a and Fig. 3b, are fully reported in Table C1.

From a quantitative point of view (see Table C1), characteristic GE-1 lengths obtained from fitting  $\sigma_{xx}$  and  $\sigma_{yy}$  are very similar,  $\ell_I \sim \ell_{II} \sim 0.55a_0$ . The values for  $\sigma_{xy}$  deviate from this behavior ( $\ell_I \sim 0.23a_0$  and  $\ell_{II} \sim 0.48a_0$ ). Nevertheless, by using the value obtained for the other components,  $\sigma_{xy}$  actually shows a very similar profile with respect to the maximum and minimum values as well as the decay far from

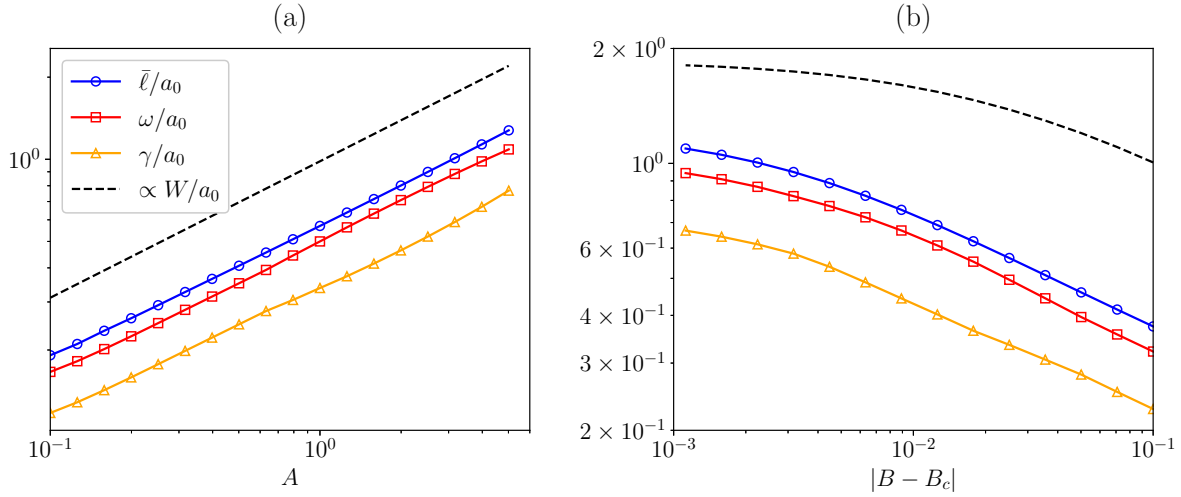


**Figure 4.** Variation of characteristic lengths with (a)  $A$  for  $B = 0.02$ , and (b)  $B$  for  $A = 1$ . In all simulations,  $C = -1/2$  and  $D = 1/3$ . The panels illustrate in particular log-log plots of  $\bar{\ell} = (\ell_I + \ell_{II})/2$  (blue circles),  $\omega$  (red squares) and  $\gamma$  (orange triangles). Solid lines are guidelines for the eyes. Values reported here are obtained by fitting  $\sigma_{yy}$ . Dependence on  $B$  is illustrated via the quenching depth  $|B - B_c|$ . The correlation length  $W$  from Eq. (C.1) is reported for comparison (dashed line).

the core. A small difference is observed only very close to the core, where the two significantly different lengths allow for smaller gradients and a better matching of the simulation results. When enforcing a single characteristic length ( $\ell_1 = \ell_2$ )—which we note in passing would again be consistent with the conclusion of lattice theory with central force interaction between atoms [67, 72]—the fitted values are very similar (see the third line in Table C1). Therefore, this deviation results from the larger number of degrees of freedom in the model and shows that GE-1 can match the simulations well but with characteristic lengths that are not fully consistent among different stress-field components. Conversely, the values obtained via fitting the characteristic GE-2 lengths are very close to each other in all three stress components, assessing that the underlying model accurately describes simulation results. By relaxing the assumption of constant magnitude of the amplitudes  $\eta_j$  underlying the derivation in Sect 3.3, we indeed find that additional contributions appear, including terms entering GE-2. Further details to substantiate this argument are reported in Appendix D.

The agreement between the simulated and analytical GE stress fields, as well as more detailed considerations above, is found to be valid across a broad parameter range. This is first shown in Fig. 3c where we report 2D stress maps and contour lines of  $\sigma_{xx}$  for three simulations featuring  $A$  or  $B$  values different from those in Fig. 3a. The change in the  $\sigma_{xx}$  is reflected in a variation of the characteristic lengths determined by fitting. This aspect is further quantitatively illustrated in Fig. 4, also allowing for further comparisons between the considered GE theories. Therein, we discuss the values of fitted characteristic lengths from  $\sigma_{yy}$ . This component is chosen as it features an almost symmetric profile owing to lower maximum values for the stress field and thus a limited

contribution of nonlinearities compared to  $\sigma_{xx}$  (see also Fig. 3). For GE-1 we show the average of the two characteristic lengths,  $\bar{\ell} = (\ell_I + \ell_{II})/2$ . Consistent with the values in Table 1 (for the simulation illustrated in Fig. 3a-b), the relative difference between their values is however below 5% over the whole range of parameters considered. For GE-2 we report the two characteristic lengths  $\omega = \sqrt{\varrho_I^2 + \varrho_{II}^2}$  and  $\gamma = \sqrt[4]{\varrho_I^2 \varrho_{II}^2}$ , allowing for direct comparisons with GE-1. We vary in particular parameters  $A$  (Fig. 4a) and  $B$  (Fig. 4b). The variation with  $B$  is illustrated in terms of the quenching depth, namely  $|B - B_c|$  with  $B_c = 8C^2/(135D)$  the value of  $B$  at which ordered (periodic  $\psi$  with triangular symmetry) and disordered (constant  $\psi$ ) phases have the same energy [47]. We note that the parameter range includes most variations typically considered for PFC models.

We generally find that effective GE lengths are larger than the one computed in Sect. 3 and also better approach common values reported in the literature for GE length scales [17, 74]. They approach values obtained in Sect. 3 for small  $A$  and  $B$ . Characteristic lengths of GE-1 and GE-2 vary similarly. Interestingly,  $\omega \sim 0.9\bar{\ell}$ . We remark that  $\omega$  is the characteristic length to the lowest order of GE-2, which reduces to GE-1. Still, these values do not match exactly and, indeed,  $\gamma \neq 0$ . Therefore, we assess further the presence of higher-order corrections from terms peculiar to GE-2, as suggested by the argument in Appendix D.

Importantly, the characteristic lengths are found to be proportional to the correlation length  $W$ . In the considered models, this quantity can be determined as the width of the interface between an ordered and disordered phase, both in equilibrium and nonequilibrium settings [78]. For the one-mode approximation of the triangular lattice, it has an analytic solution, reported in Eq. (C.1). The same or slightly varying proportionality constant over the whole range of explored parameters is obtained, namely  $\bar{\ell}/W \sim \omega/W \in (0.4, 0.6)$ . We remark, however, that the expression of  $W$  used here, Eq. (C.1), is also derived in an approximated setting. In models like SH or PFC, the extension of the defect core is also found to scale similarly with the correlation length [79]. Therefore, the effective characteristic length is found to scale *de facto* with the core size, consistent with continuum descriptions of the elastic field of dislocations in GE theories [20, 21, 23]. Importantly, by recalling that  $B$  is a phenomenological temperature parameter, the effective GE characteristic lengths at dislocations are then found to be connected to the temperature.

## 6. Conclusion

We discussed how gradient elasticity (GE) is encoded in Swift-Hohenberg (SH) and phase-field crystal (PFC) models. At leading order for small deformations, it consists of a first strain-gradient elasticity formulation, anisotropic for stripe phases and isotropic for crystalline phases. We derived analytical or semi-analytical formulations for GE characteristic lengths for one and multimode approximations of the periodic order parameter for different crystalline arrangements in a simplified setting. Moreover, we outlined the possibility of extending the parametrization via the design of the nonlocal



terms in the free energy.

The computed characteristic lengths are in the order of fractions of the lattice parameter, i.e., in the order of  $1\text{\AA}$  as observed for several materials. From a quantitative point of view, they are consistent with results reported in the literature, although they underestimate the ones commonly found for real materials with the same lattice symmetries [17, 74]. Moreover, in the minimal formulation of SH and PFC models, they can only be slightly varied, conforming to the known restrictions on the tuning of elastic constants in these approaches.

However, numerical simulations which inherently encode a coarse-graining over microscopic lengths and do not consider any approximation, show that larger effective GE characteristic lengths emerge. They can be significantly varied with the model parameters. In particular, we focused on the elastic field at dislocations, which is of central interest for both GE and SH/PFC models. Interestingly, the solution of dislocation fields in both first and second strain-gradient elasticity can be fitted well to the results of APFC simulations. By analyzing the values of the emerging effective characteristic lengths, we found GE-2 to be a better model for describing the simulated stress field, thus assessing the underlying GE theory. Overall, we established that these theories are suitable for reproducing the elastic field of dislocations within the considered models, including regularization at the dislocation cores. On the other hand, we show that these GE theories naturally emerge from the minimal framework of the SH energy functional, which can be considered the simplest free-energy form minimized by a periodic, smooth order parameter [32].

The effective GE characteristic lengths at dislocations vary with the model parameters similarly to the correlation length. This closely resembles variations observed for the size of defect cores in smooth theories for ordered systems [79]. Importantly, the variation in the quenching depth can be interpreted as a dependence on temperature. Thanks to the derivation from SH and PFC models, GE is directly linked to a framework for order-disorder phase transition. The dependence on quenching depth may constitute the input for other theories.

## **Acknowledgements**

We acknowledge interesting discussions with Ken R. Elder, Markus Lazar, and Axel Voigt. We also gratefully acknowledge support from the German Research Foundation under Grant No. SA4032/2 – Emmy Noether Programme – (MS) and SA4032/3 – FOR3013 – (LMB), and from the Center for Information Services and High-Performance Computing [Zentrum für Informationsdienste und Hochleistungsrechnen (ZIH)] at TU Dresden for computing time.

## Data Availability Statement

The data that support the findings of this study are openly available at the following URL/DOI: *<Information provided in the next version>*.

## Appendix A. Numerical Method

Numerical simulations are computed by exploiting a Fourier pseudo-spectral method. In brief, we solve the equation(s) (35) rewritten as

$$\partial_t \eta_n = \mathfrak{L} \eta_n + \mathfrak{N}(\{\eta_n\}), \quad (\text{A.1})$$

with  $\eta_n$  the amplitudes to solve for,  $\mathfrak{L}$  the linear operator in  $\eta_n$  of Eq. (35), and  $\mathfrak{N}$  the nonlinear part. We recall that the latter includes nonlinear terms in all the amplitudes  $\eta_n$ . In the Fourier pseudo-spectral method, we then solve for

$$\partial_t [\hat{\eta}_n]_k = \hat{\mathfrak{L}}_k [\hat{\eta}_n]_k + \hat{\mathfrak{N}}_k, \quad (\text{A.2})$$

with  $[\hat{\eta}_n]_k$  the coefficient of the Fourier transform of  $\eta_n$ ,  $\hat{\mathfrak{N}}_k$  the Fourier transform of  $\mathfrak{N}(\{\eta_n\})$  and  $\hat{\mathfrak{L}}_k$  the Fourier transform of  $\mathfrak{L}$  resulting in an algebraic expression of the wave vector (for instance, in 1D, for  $\mathfrak{L}\eta = \frac{\partial^2 \eta}{\partial x^2}$  one gets  $\hat{\mathfrak{L}}_k = -k^2$  with  $k$  the coordinate in the Fourier space). The solution at  $t + \Delta t$ , with  $\Delta t$  the timestep, is then obtained via an inverse Fourier transform of  $[\hat{\eta}_n]_k(t + \Delta t)$  computed by the following approximation

$$[\hat{\eta}_n]_k(t + \Delta t) \approx e^{\mathfrak{L}_k \Delta t} [\hat{\eta}_n]_k(t) + \frac{e^{\mathfrak{L}_k \Delta t} - 1}{\mathfrak{L}_k} \hat{\mathfrak{N}}_k(t). \quad (\text{A.3})$$

This method enforces periodic boundary conditions. We implemented it in `python` (code openly available, see [82]). An established Fast-Fourier Transform algorithm (FFTW) is exploited [83]. We use a discretization of 4 mesh points per atomic site with a timestep  $\Delta t = 1$ .

From  $\{\eta_n\}$  computed with the method outlined above, we compute the stress field components. This is achieved via the equation [50]

$$\begin{aligned} \sigma_{ij} = \sum_m^M \left\{ [(\partial_i + i(\mathbf{k}_m)_i)(\nabla^2 + 2i\mathbf{k}_m \cdot \nabla)\eta_m] [(\partial_j - i(\mathbf{k}_m)_j)\eta_m^*] \right. \\ \left. - [(\nabla^2 + 2i\mathbf{k}_m \cdot \nabla)\eta_m] [(\partial_i - i(\mathbf{k}_m)_i)(\partial_j - i(\mathbf{k}_m)_j)\eta_m^* + \text{c.c.}] \right\}, \end{aligned} \quad (\text{A.4})$$

## Appendix B. Stress field of an edge dislocation in strain-gradient elasticity

In Toupin-Mindlin first strain-gradient elasticity (GE-1, Sect. 2.1), the stress field in the  $xy$ -plane for an edge dislocation located at the origin with Burgers vector aligned with



the  $x$ -axis,  $\mathbf{b} = b_x \hat{\mathbf{x}}$ , reads [23]:

$$\begin{aligned} \sigma_{xx} = -\sigma_0 \frac{y}{r^2} & \left\{ \frac{3x^2 + y^2}{r^2} - \frac{2\nu r}{\ell_1} K_1(r/\ell_1) \right. \\ & + (1 - 2\nu) \left[ \frac{3x^2 - y^2}{r^2} \left( \frac{4\ell_1^2}{r^2} - 2K_2(r/\ell_1) \right) - \frac{2x^2}{\ell_1 r} K_1(r/\ell_1) \right] \\ & \left. - 2(1 - \nu) \left[ \frac{3x^2 - y^2}{r^2} \left( \frac{4\ell_2^2}{r^2} - 2K_2(r/\ell_2) \right) - \frac{x^2 - y^2}{\ell_2 r} K_1(r/\ell_2) \right] \right\}, \end{aligned} \quad (\text{B.1})$$

$$\begin{aligned} \sigma_{yy} = \sigma_0 \frac{y}{r^2} & \left\{ \frac{x^2 - y^2}{r^2} + \frac{2\nu r}{\ell_1} K_1(r/\ell_1) \right. \\ & + (1 - 2\nu) \left[ \frac{3x^2 - y^2}{r^2} \left( \frac{4\ell_1^2}{r^2} - 2K_2(r/\ell_1) \right) + \frac{2y^2}{\ell_1 r} K_1(r/\ell_1) \right] \\ & \left. - 2(1 - \nu) \left[ \frac{3x^2 - y^2}{r^2} \left( \frac{4\ell_2^2}{r^2} - 2K_2(r/\ell_2) \right) - \frac{x^2 - y^2}{\ell_2 r} K_1(r/\ell_2) \right] \right\}, \end{aligned} \quad (\text{B.2})$$

$$\begin{aligned} \sigma_{xy} = \sigma_0 \frac{x}{r^2} & \left\{ \frac{x^2 - y^2}{r^2} \right. \\ & + (1 - 2\nu) \left[ \frac{x^2 - 3y^2}{r^2} \left( \frac{4\ell_1^2}{r^2} - 2K_2(r/\ell_1) \right) + \frac{2y^2}{\ell_1 r} K_1(r/\ell_1) \right] \\ & \left. - 2(1 - \nu) \left[ \frac{x^2 - 3y^2}{r^2} \left( \frac{4\ell_2^2}{r^2} - 2K_2(r/\ell_2) \right) + \frac{2y^2}{\ell_2 r} K_1(r/\ell_2) \right] \right\}, \end{aligned} \quad (\text{B.3})$$

with  $\sigma_0 = (\mu b_x)/(2\pi(1-\nu))$ ,  $r = \sqrt{x^2 + y^2}$ , and  $K_n(x)$  are the modified Bessel functions of the second kind ( $n = 1, 2$  here). The classical (singular) stress field obtained in linear elasticity is recovered for  $\ell_1 = \ell_2 = \ell \rightarrow 0$  [24].

In the special second strain-gradient elasticity theory (GE-2) outlined in Sect. 2.3, the stress field components for the same dislocation read [21]

$$\begin{aligned} \sigma_{xx} = -\sigma_0 \frac{y}{r^4} & \left\{ (y^2 + 3x^2) + \frac{4(\varrho_1^2 + \varrho_2^2)}{r^2} (y^2 - 3x^2) - \frac{2ry^2}{\varrho_1^2 - \varrho_2^2} \left[ \varrho_1 K_1\left(\frac{r}{\varrho_1}\right) - \varrho_2 K_1\left(\frac{r}{\varrho_2}\right) \right] \right. \\ & \left. - \frac{2(y^2 - 3x^2)}{\varrho_1^2 - \varrho_2^2} \left[ \varrho_1^2 K_2\left(\frac{r}{\varrho_1}\right) - \varrho_2^2 K_2\left(\frac{r}{\varrho_2}\right) \right] \right\}, \end{aligned} \quad (\text{B.4})$$

$$\begin{aligned} \sigma_{yy} = -\sigma_0 \frac{y}{r^4} & \left\{ (y^2 - x^2) - \frac{4(\varrho_1^2 + \varrho_2^2)}{r^2} (y^2 - 3x^2) - \frac{2rx^2}{\varrho_1^2 - \varrho_2^2} \left[ \varrho_1 K_1\left(\frac{r}{\varrho_1}\right) - \varrho_2 K_1\left(\frac{r}{\varrho_2}\right) \right] \right. \\ & \left. + \frac{2(y^2 - 3x^2)}{\varrho_1^2 - \varrho_2^2} \left[ \varrho_1^2 K_2\left(\frac{r}{\varrho_1}\right) - \varrho_2^2 K_2\left(\frac{r}{\varrho_2}\right) \right] \right\}, \end{aligned} \quad (\text{B.5})$$

$$\begin{aligned} \sigma_{xy} = \sigma_0 \frac{x}{r^4} & \left\{ (x^2 - y^2) - \frac{4(\varrho_1^2 + \varrho_2^2)}{r^2} (x^2 - 3y^2) - \frac{2ry^2}{\varrho_1^2 - \varrho_2^2} \left[ \varrho_1 K_1\left(\frac{r}{\varrho_1}\right) - \varrho_2 K_1\left(\frac{r}{\varrho_2}\right) \right] \right. \\ & \left. + \frac{2(x^2 - 3y^2)}{\varrho_1^2 - \varrho_2^2} \left[ \varrho_1^2 K_2\left(\frac{r}{\varrho_1}\right) - \varrho_2^2 K_2\left(\frac{r}{\varrho_2}\right) \right] \right\}. \end{aligned} \quad (\text{B.6})$$

An illustration of the stress field components for GE-1, GE-2, and the continuum elasticity limit CE, is reported in Fig. B1.

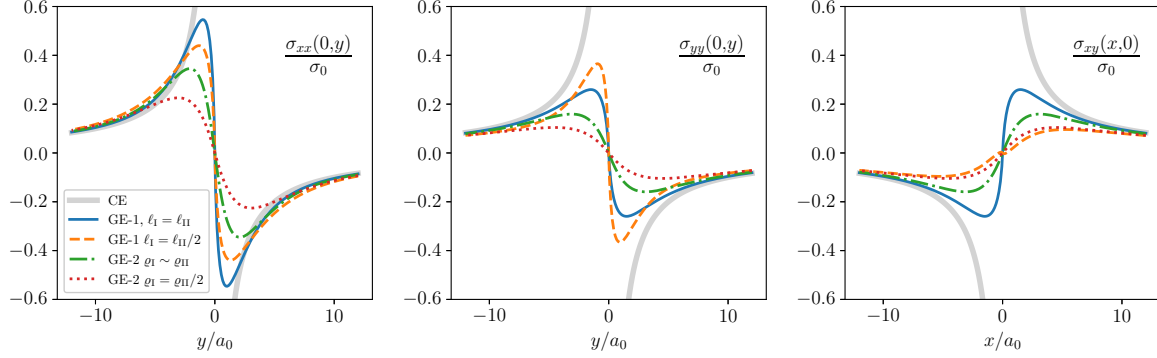


**Figure B1.** Stress field components  $\sigma_{xx}$ ,  $\sigma_{yy}$ , and  $\sigma_{xy}$  (left to right) from GE-1 and GE-2, namely Eqs. (B.1)–(B.3) [23] and (B.4)–(B.6) [21], respectively. Two ratios for characteristic lengths are showcased, where  $\ell_1 = \varrho_1 = 1$ . The linear continuum elasticity solution (CE) [24] is obtained with Eqs. (B.1)–(B.3) in the limit  $\ell_1 = \ell_2 \rightarrow 0$ .

## Appendix C. Details of fitting procedures for characteristic lengths

The equations reported in Appendix B, upon centering the frame of reference at the dislocation core in  $(x_0, y_0)$ , illustrate functions  $\sigma_{ij}(x, y, x_0, y_0, E, \nu, \xi_1, \xi_2)$  with  $\xi_i = \ell_i$  for GE-1 and  $\xi_i = \varrho_i$  for GE-2. These are here fitted (exploiting `scipy.optimize` [84]) on  $\sigma_{ij}(x, y)$  in a squared region  $15a_0 \times 15a_0$  centered on a defect to determine  $\xi_i$ . Exploiting the elastic constants obtained in Table 1, and in agreement with [40, 61], we have that for the one-mode approximation of the triangular lattice the Lamé constants read  $\mu = \lambda = 3A\varphi_1^2$ , which results in the Young modulus  $E = 5A\varphi_1^2/2$  and Poisson ratio  $\nu = 1/4$  (under the plane strain assumption).  $\varphi$  can be computed analytically for one-mode approximations [47]. The value for the considered triangular lattice is  $\varphi = (-C + \sqrt{C^2 - 15BD})/(15D)$ . The dislocation in the APFC simulations moves slightly upon reaching equilibrium. In general,  $x_0$  and  $y_0$  are then to be considered as fitting parameters as well. The fit results for the fields illustrated in Fig. 3 are reported in Table C1. The fitted values of the characteristic lengths  $\ell_i$  and  $\varrho_i$  are indicated with the subscripts “I” and “II”.

The values of fitted parameters are overall consistent across different stress components, with just GE-1 characteristic lengths obtained by fitting  $\sigma_{xy}$  deviating from other components, as discussed in the main text. Note that  $x_0$  differs from 0 by less than 5% of the lattice parameter. The shift along the  $x$  direction could then be considered negligible. Instead, we obtain a shift along  $y$  of  $\sim 20\%$  of the lattice parameter. Note that the dislocation core location  $(x_0, y_0)$  is quantitatively consistent also when looking at the fitted values on both GE-1 and GE-2 stress field components, where indeed  $x_0$  and  $y_0$  have the same meaning. In the plots reported in the main text,

	$\sigma_{xx}$	$\sigma_{yy}$	$\sigma_{xy}$	Average
$\ell_I$	0.5413	0.5600	0.2275	0.4429
$\ell_{II}$	0.5800	0.5789	0.4303	0.5290
$\ell_I = \ell_{II}$	0.5630	0.5597	0.5692	0.5640
$\varrho_I$	0.4472	0.4227	0.4275	0.4325
$\varrho_{II}$	0.2415	0.2673	0.2746	0.2612
$x_0^{\text{GE-1}}$	-0.0216	0.0072	0.0450	0.0101
$x_0^{\text{GE-2}}$	-0.0204	0.0065	0.0452	0.0104
$y_0^{\text{GE-1}}$	-0.2079	-0.1951	-0.2088	-0.2039
$y_0^{\text{GE-2}}$	-0.2000	-0.1839	-0.21103	-0.1983

**Table C1.** Results of the fits illustrated in Fig. 3(a). Values  $(\ell_I, \ell_{II}, x_0^{\text{GE-1}}, y_0^{\text{GE-1}})$  are obtained by fitting Eqs (B.1)–(B.3) with characteristic lengths and positions as fitting parameters. The values  $\ell_I = \ell_{II}$  are obtained from fitting the same equation but enforcing this constraint. Values  $(\varrho_I, \varrho_{II}, x_0^{\text{GE-2}}, y_0^{\text{GE-2}})$  are obtained by fitting Eqs (B.4)–(B.6), also in this case with characteristic lengths and positions as fitting parameters. All quantities are expressed in  $a_0$  units (fraction of the lattice parameter). For all these values, the standard deviation does not exceed  $2 \times 10^{-4}$ .

the stress fields from GE solutions for dislocations are centered in the  $(x_0, y_0)$  values obtained from fitting the corresponding stress component. We remark that in GE-2, the two length scales  $\varrho_{1,2}$  are fully equivalent as it follows from Eq. (23), so their values could be exchanged. Also, in some parameter ranges, e.g., for small  $A$  values, the best fit is given by  $\varrho_1 \sim \varrho_2$  while in other cases a significant difference, as in the Table above, is obtained. The physically meaningful lengths entering the theory are, however,  $\omega(\varrho_1, \varrho_2)$  and  $\gamma(\varrho_1, \varrho_2)$  as defined in Sect. 2.3 and these are the quantities illustrated in Fig. 4. In this figure, we also report the correlation length  $W$  for triangular lattice when varying  $A$  and  $B$ . For this lattice symmetry in the one-mode approximation, an analytic solution connecting  $W$  to the model parameter exists [78]

$$W(A, B) = \sqrt{\frac{A}{|B|}} \frac{4\sqrt{2}}{\zeta + \sqrt{\zeta^2 - 4\iota}}, \quad (\text{C.1})$$

with  $\iota = \mp 1$  for  $B \lessgtr 0$  and  $\zeta = 2C/\sqrt{15|B|D}$ .

## Appendix D. On higher order GE terms from nonconstant amplitudes

The main text discusses evidence of second-strain gradient elasticity contributions in numerical simulations. In particular, the stress field at the dislocation core and the detailed analysis by comparison with analytic solutions within GE-1 and GE-2 show that the latter better describes the simulation results.

In Sect. 3, we show that under the assumption of constant magnitude of the amplitude ( $|\nabla\varphi_n| = 0$ ) typically considered for small deformations, GE is encoded in the SH energy functional via first strain-gradient terms only. This assumption, however, does not strictly hold true in simulations [45, 80, 81]. While refraining from a complete derivation of the theory, we report here a simplified argument to show how including the amplitude gradients leads to second strain-gradient terms in the elastic energy.

In one spatial dimension, by assuming that the gradient of the amplitude is of the same order as the gradient of the displacement while still ignoring all higher-order nonlinear terms as in Sect. 3, the elastic energy density reads:

$$\begin{aligned} \frac{w}{A'} = & k^2 [4k^2 u'(x)^2 + u''(x)^2] \varphi(x) + 4k^2 [\varphi'(x) - \varphi(x) u''(x)] \varphi'(x) \\ & + [\varphi''(x) + 4k^2 \varphi(x) u'(x)] \varphi''(x). \end{aligned} \quad (\text{D.1})$$

Minimizing this expression with respect to the amplitude  $\varphi(x)$ , we obtain:

$$\varphi''(x) = \left\{ \frac{B + 3D\varphi(x)^2}{A'(1 + 4k^2)} + \frac{A'k^2}{A'(1 + 4k^2)} [4k^2 u'(x)^2 - (2 - u''(x))u''(x) + 2u'''(x)] \right\} \varphi(x). \quad (\text{D.2})$$

Therefore,  $\varphi''(x)$  and, by extension, the elastic energy density, contain a contribution from  $u'''(x)$ , i.e. the second derivative of the strain field, which is the higher-order term entering GE-2 but absent in GE-1. As such, GE-2 effects may be ascribed to gradients in the amplitude, while their presence is anyhow corroborated by numerical results and, importantly, a detailed comparison with specific analytical solutions.

## References

- [1] Toupin R 1962 *Arch. Ration. Mech. Anal.* **11** 385–414
- [2] Toupin R A 1964 *Arch. Ration. Mech. Anal.* **17** 85–112
- [3] Mindlin R D 1964 *Arch. Ration. Mech. Anal.* **16** 51–78
- [4] Mindlin R and Eshel N 1968 *Int. J. Solids Struct.* **4** 109 – 124
- [5] Askes H and Aifantis E C 2011 *Int. J. Solids Struct.* **48** 1962–1990
- [6] Lam D, Yang F, Chong A, Wang J and Tong P 2003 *J. Mech. Phys. Solids* **51** 1477–1508
- [7] Zhang X and Sharma P 2005 *Int. J. Solids Struct.* **42** 3833–3851
- [8] Gao X L and Park S 2007 *Int. J. Solids Struct.* **44** 7486–7499
- [9] Akgöz B and Civalek Ö 2011 *Curr. Appl. Phys.* **11** 1133–1138
- [10] Po G, Lazar M, Seif D and Ghoniem N 2014 *J. Mech. Phys. Solids* **68** 161–178
- [11] Mao S and Purohit P K 2014 *J. Appl. Mech.* **81** 081004
- [12] Jiang Y, Li L and Hu Y 2022 *Acta Mechanica* **233** 3213–3231
- [13] Fleck N, Muller G, Ashby M F and Hutchinson J W 1994 *Acta Metall. Mater.* **42** 475–487
- [14] Gao H, Huang Y, Nix W and Hutchinson J 1999 *J. Mech. Phys. Solids* **47** 1239–1263

- [15] Hutchinson J and Fleck N 1997 *Adv. Appl. Mech.* **33** 295–361
- [16] Fleck N and Hutchinson J 2001 *J. Mech. Phys. Solids* **49** 2245–2271
- [17] Shodja H, Zaheri A and Tehranchi A 2013 *Mech. Mater.* **61** 73–78
- [18] Admal N C, Marian J and Po G 2017 *J. Mech. Phys. Solids* **99** 93–115
- [19] Po G, Admal N C and Lazar M 2019 *Mater. Theory* **3** 1–16
- [20] Lazar M and Maugin G A 2005 *Int. J. Eng. Sci.* **43** 1157–1184
- [21] Lazar M, Maugin G A and Aifantis E C 2006 *Int. J. Solids Struct.* **43** 1787–1817
- [22] Lazar M 2013 *Int. J. Solids Struct.* **50** 352 – 362
- [23] Lazar M 2022 *Contin. Mech. Thermodyn.* **34** 1433–1454
- [24] Anderson P, Hirth J and Lothe J 2017 *Theory of Dislocations* (Cambridge University Press) ISBN 9780521864367
- [25] Müller P and Saúl A 2004 *Surf. Sci. Rep.* **54** 157–258
- [26] Genzer J and Groenewold J 2006 *Soft Matter* **2** 310–323
- [27] Swift J and Hohenberg P C 1977 *Phys. Rev. A* **15** 319–328
- [28] Cross M C and Hohenberg P C 1993 *Rev. Mod. Phys.* **65** 851–1112
- [29] Aranson I S and Tsimring L S 2006 *Rev. Mod. Phys.* **78** 641
- [30] Stoop N, Lagrange R, Terwagne D, Reis P M and Dunkel J 2015 *Nat. Mater.* **14** 337–342
- [31] Oza A U, Heidenreich S and Dunkel J 2016 *Eur. Phys. J. E* **39** 1–8
- [32] Elder K R, Katakowski M, Haataja M and Grant M 2002 *Phys. Rev. Lett.* **88** 245701
- [33] Elder K R and Grant M 2004 *Phys. Rev. E* **70** 051605
- [34] Provatas N and Elder K 2010 *Phase-Field Methods in Materials Science and Engineering* (Wiley-VCH Verlag GmbH) ISBN 9783527631520
- [35] Emmerich H, Löwen H, Wittkowski R, Gruhn T, Tóth G I, Tegze G and Gránásy L 2012 *Adv. Phys.* **61** 665–743
- [36] Berry J, Provatas N, Rottler J and Sinclair C W 2014 *Phys. Rev. B* **89** 214117
- [37] Backofen R, Barmak K, Elder K R and Voigt A 2014 *Acta Mater.* **64** 72
- [38] Gránásy L, Tóth G I, Warren J A, Podmaniczky F, Tegze G, Rátkai L and Pusztai T 2019 *Prog. Mater. Sci.* **106** 100569
- [39] Trautt Z, Adland A, Karma A and Mishin Y 2012 *Acta Mater.* **60** 6528–6546
- [40] Heinonen V, Achim C V, Elder K R, Buyukdagli S and Ala-Nissila T 2014 *Phys. Rev. E* **89** 032411
- [41] Stefanovic P, Haataja M and Provatas N 2006 *Phys. Rev. Lett.* **96** 225504
- [42] Tóth G I, Gránásy L and Tegze G 2013 *J. Phys. Cond. Matter* **26** 055001
- [43] Heinonen V, Achim C V, Kosterlitz J M, Ying S C, Lowengrub J and Ala-Nissila T 2016 *Phys. Rev. Lett.* **116** 024303
- [44] Skogvoll V, Skaugen A, Angheluta L, Salvalaglio M and Viñals J 2022 *J. Mech. Phys. Solids* **166** 104932
- [45] Hüter C, Friák M, Weikamp M, Neugebauer J, Goldenfeld N, Svendsen B and Spatschek R 2016 *Phys. Rev. B* **93** 214105
- [46] Hüter C, Neugebauer J, Boussinot G, Svendsen B, Prahl U and Spatschek R 2017 *Contin. Mech. Thermodyn* **29** 895–911
- [47] Salvalaglio M and Elder K R 2022 *Model. Simul. Mater. Sci. Eng.* **30** 053001
- [48] Skaugen A, Angheluta L and Viñals J 2018 *Phys. Rev. B* **97** 054113
- [49] Salvalaglio M, Voigt A and Elder K R 2019 *npj Comput. Mater.* **5** 48
- [50] Salvalaglio M, Angheluta L, Huang Z f, Voigt A, Elder K R and Viñals J 2020 *J. Mech. Phys. Solids* **137** 103856
- [51] Ramakrishnan T V and Yussouff M 1979 *Phys. Rev. B* **19** 2775–2794
- [52] Evans R 1979 *Adv. Phys.* **28** 143–200
- [53] Singh Y 1991 *Phys. Rep.* **207** 351–444
- [54] Elder K R, Provatas N, Berry J, Stefanovic P and Grant M 2007 *Phys. Rev. B* **75** 064107
- [55] van Teeffelen S, Backofen R, Voigt A and Löwen H 2009 *Phys. Rev. E* **79** 051404
- [56] Archer A J, Ratliff D J, Rucklidge A M and Subramanian P 2019 *Phys. Rev. E* **100** 022140

- [57] Greenwood M, Provatas N and Rottler J 2010 *Phys. Rev. Lett.* **105** 045702
- [58] Greenwood M, Rottler J and Provatas N 2011 *Phys. Rev. E* **83** 031601
- [59] Mkhonta S K, Elder K R and Huang Z F 2013 *Phys. Rev. Lett.* **111** 035501
- [60] Spatschek R and Karma A 2010 *Phys. Rev. B* **81** 214201
- [61] Elder K R, Huang Z F and Provatas N 2010 *Phys. Rev. E* **81** 011602
- [62] Goldenfeld N, Athreya B P and Dantzig J A 2005 *Phys. Rev. E* **72** 020601
- [63] Athreya B P, Goldenfeld N and Dantzig J A 2006 *Phys. Rev. E* **74** 011601
- [64] Yeon D H, Huang Z F, Elder K and Thornton K 2010 *Philos. Mag.* **90** 237–263
- [65] De Donno M, Benoit-Maréchal L and Salvalaglio M 2023 *Phys. Rev. Mater.* **7** 033804
- [66] Hermann C 1934 *Zeitschrift für Kristallographie - Crystalline Materials* **89** 32–48
- [67] Lazar M, Agiasofitou E and Böhlke T 2022 *Contin. Mech. Thermodyn.* **34** 107–136
- [68] Elder K R, Viñals J and Grant M 1992 *Phys. Rev. Lett.* **68** 3024–3027
- [69] Elder K R, Viñals J and Grant M 1992 *Phys. Rev. A* **46** 7618–7629
- [70] Praetorius S, Voigt A, Wittkowski R and Löwen H 2018 *Phys. Rev. E* **97** 052615
- [71] Huang Z F, Löwen H and Voigt A 2022 *Commun. Phys.* **5** 294
- [72] Born M, Huang K and Lax M 1955 *American Journal of Physics* **23** 474–474
- [73] Zhang X, Jiao K, Sharma P and Yakobson B 2006 *J. Mech. Phys. Solids* **54** 2304–2329
- [74] Lazar M and Agiasofitou E 2023 *PAMM* **23** e202300121
- [75] Jaatinen A, Achim C V, Elder K R and Ala-Nissila T 2009 *Phys. Rev. E* **80** 031602
- [76] Ofori-Opoku N, Stolle J, Huang Z F and Provatas N 2013 *Phys. Rev. B* **88** 104106
- [77] Skogvoll V, Skaugen A and Angheluta L 2021 *Phys. Rev. B* **103** 224107
- [78] Galenko P, Sanches F I and Elder K 2015 *Phys. D: Nonlinear Phenom.* **308** 1–10
- [79] Skogvoll V, Rønning J, Salvalaglio M and Angheluta L 2023 *npj Comput. Mater.* **9** 122
- [80] Wang Z L, Huang Z F and Liu Z 2018 *Phys. Rev. B* **97** 144112
- [81] Ainsworth M and Mao Z 2019 *Physical Review B* **100** 104101
- [82] Gitlab repository URL <https://gitlab.com/3ms-group/apfc-fft-ge>
- [83] Frigo M and Johnson S 2005 *Proceedings of the IEEE* **93** 216–231
- [84] Virtanen P *et al* 2020 *Nature Methods* **17** 261–272